Ditin(IV) Chalcogenide Anions: ^{77}Se, ^{119}Sn, and ^{125}Te Solution NMR Study of the $Sn_2Ch_6^{4-}$ and $Sn_2Ch_7^{4-}$ (Ch = Se, Te) Anions, X-ray Crystal Structures and Raman Spectra of $K^+(N(CH_3)_4^+)_3Sn_2Se_6^{4-}$, $(enH^+)_2(2,2,2\text{-crypt-}K^+)_2Sn_2Se_6^{4-}$, and $(K^+)_2(2,2,2\text{-crypt-}K^+)_2Sn_2Te_6^{4-}$, and X-ray Crystal Structures of $K^+(2,2,2\text{-crypt-}K^+)_2HOSnTe_3^{3-}$ and $K^+(2,2,2\text{-crypt-}K^+)_2HOSnTe_3^{3-}\cdot en$

Janette Campbell, Lesley A. Devereux, Michael Gerken, Hélène P. A. Mercier, Ayaaz M. Pirani, and Gary J. Schrobilgen*

Department of Chemistry, McMaster University, Hamilton, Ontario L8S 4M1, Canada

Received July 27, 1995[⊗]

The seleno- and tellurostannate(IV) anions $Sn_2Ch_6^{4-}$ and $Sn_2Ch_7^{4-}$ (Ch = Se, Te) have been obtained by extraction of the ternary alloys $KSn_{0.67}Se_{1.93}$ and $KSn_{0.63}Te_{1.70}$ in ethylenediamine (en) and/or liquid NH_3 in the absence and in the presence of nonstoichiometric amounts of 2,2,2-crypt (4,7,13,16,21,24-hexaoxa-1,10-diazabicyclo[8.8.8]-hexacosane) with respect to K^+. The anions were characterized in solution for the first time by natural abundance ^{77}Se, ^{119}Sn, and ^{125}Te NMR spectroscopy. The magnitudes of the relativistically corrected reduced coupling constants $^1K(Sn-Ch_t)_{RC}$, $^1K(Sn-Ch_{mb})_{RC}$, and $^1K(Sn-Ch_{db})_{RC}$ were shown to be consistent with a significant degree of s-character in the bonding. The $Sn-Ch_{mb}$ and $Sn-Ch_t$ bond distances observed for the dimeric $SnCh_3^{2-}$ anions, namely $Sn_2Ch_6^{4-}$, in $K^+(N(CH_3)_4^+)_3Sn_2Se_6^{4-}$ (**1**), $(enH^+)_2(2,2,2\text{-crypt-}K^+)_2Sn_2Se_6^{4-}$ (**2**), and $(K^+)_2(2,2,2\text{-crypt-}K^+)_2Sn_2Te_6^{4-}$ (**3**) were shown to correlate with the $^1K(Sn-Ch)_{RC}$ values, indicating that the solid-state molecular structures of the anions are retained in solution. The Raman spectra of compounds **1**−**3** are also reported along with their respective factor-group analyses. The novel $HOSnTe_3^{3-}$ anion, the hydroxide derivative of the $SnTe_3^{2-}$ anion, has been structurally characterized by X-ray crystallography in $K^+(2,2,2\text{-crypt-}K^+)_2$-$HOSnTe_3^{3-}$ (**4**) and in $K^+(2,2,2\text{-crypt-}K^+)_2HOSnTe_3^{3-}\cdot en$ (**5**) and represents the first example of a simple mixed hydroxychalcogenide anion of tin.

Introduction

Although the chemistry of transition-metal polysulfide,[1−6] polyselenide,[4,7−12] and polytelluride[7−12,13] anions has been extensively reviewed in the literature, relatively little has been reported on the chemistry of the main-group-metal congeners.[4,9,11,14,15] Of the known main-group-metal chalcogenide anions, the majority have been structurally characterized by X-ray crystallography, e.g., $Ga_6Se_{14}^{10-}$,[16] $In_2Se_{21}^{4-}$,[17] $In_2S_x^{2-}$ (x = 14, 16),[18] $Tl_2Te_2^{2-}$,[19] $Ge_2Se_8^{4-}$,[20] $Pb_2Ch_3^{2-}$ (Ch = Se,[21] Te[22,23]), $Sb_{12}Se_{20}^{4-}$,[24] and $Sb_4S_6^{2-}$.[25] In contrast, only few main-group-metal chalcogenide anions have been structurally characterized by solution multi-NMR spectroscopy, even though Se, Te, and heavy main-group metals like Sn, Tl, and Pb possess readily accessible natural abundance spin $^1/_2$ nuclides, i.e., ^{77}Se, ^{125}Te, ^{117,119}Sn, ^{203,205}Tl, and ^{207}Pb. Solution multi-NMR studies of main-group-metal chalcogenides have the potential to provide corroborating structural information in the form of chemical shifts and M−Ch spin−spin coupling constants which may correlate with structural parameters and vibrational frequencies observed in the solid state.

The first classically bonded tin(IV) chalcogenide anion characterized in solution by ^{119}Sn and ^{125}Te NMR spectroscopy was the $SnTe_4^{4-}$ anion.[26] Schrobilgen and co-workers[28] subsequently characterized the complete series of classically bonded tin(IV) anions $SnSe_xTe_{4-x}^{4-}$ (x = 0−4), as well as $SnSe_xTe_{3-x}^{2-}$ (x = 0−3), by solution ^{77}Se, ^{119}Sn, and ^{125}Te NMR spectroscopy. The monomeric $SnCh_4^{4-}$ (Ch = Se,[29] Te[30]) anions have also been characterized in the solid state by X-ray crystal-

[⊗] Abstract published in *Advance ACS Abstracts,* April 1, 1996.

(1) Müller, A.; Jaegermann, W.; Enemark, J. H. *Coord. Chem. Rev.* **1982**, *46*, 245.
(2) Draganjac, M.; Rauchfuss, T. B. *Angew. Chem., Int. Ed. Engl.* **1985**, *24*, 742.
(3) Müller, A.; Diemann, E. *Adv. Inorg. Chem.* **1987**, *31*, 89.
(4) Fenske, D.; Ohmer, J.; Hachgenei, J.; Merzweiler, K. *Angew. Chem., Int. Ed. Engl.* **1988**, *27*, 1277.
(5) Wachter, J. *Angew. Chem., Int. Ed. Engl.* **1989**, *28*, 1613.
(6) Krebs, B.; Henkel, G. *Angew. Chem., Int. Ed. Engl.* **1991**, *30*, 769.
(7) Ansari, M. A.; Ibers, J. A. *Coord. Chem. Rev.* **1990**, *100*, 223.
(8) Kolis, J. W. *Coord. Chem. Rev.* **1990**, *105*, 195.
(9) Kanatzidis, M. G. *Comments Inorg. Chem.* **1990**, *10*, 161.
(10) Roof, L. C.; Kolis, J. W. *Chem. Rev.* **1993**, *93*, 1037.
(11) Kanatzidis, M. G.; Huang, S.-P. *Coord. Chem. Rev.* **1994**, *130*, 509.
(12) Dance, I.; Fisher, K. *Prog. Inorg. Chem.* **1994**, *41*, 637.
(13) Ansari, M. A.; McConnachie, J. M.; Ibers, J. A. *Acc. Chem. Res.* **1993**, *26*, 574.
(14) Krebs, B. *Angew. Chem., Int. Ed. Engl.* **1983**, *22*, 113.
(15) Drake, G. W.; Kolis, J. W. *Coord. Chem. Rev.* **1994**, *137*, 131.
(16) Deiseroth, H.-J.; Fu-Son, H. *Angew. Chem., Int. Ed. Engl.* **1981**, *20*, 962.
(17) Kanatzidis, M. G.; Dhingra, S. *Inorg. Chem.* **1989**, *28*, 2024.
(18) Dhingra, S. S.; Kanatzidis, M. G. *Inorg. Chem.* **1993**, *32*, 3300.
(19) Burns, R. C.; Corbett, J. D. *J. Am. Chem. Soc.* **1981**, *103*, 2627.
(20) Sheldrick, W. S.; Schaaf, B. *Z. Naturforsch.* **1994**, *B49*, 655.
(21) Björgvinsson, M.; Sawyer, J. F.; Schrobilgen, G. J. *Inorg. Chem.* **1987**, *26*, 741.
(22) Björgvinsson, M.; Sawyer, J. F.; Schrobilgen, G. J. *Inorg. Chem.* **1991**, *30*, 2231.
(23) Park, C.-W.; Salm, R. J.; Ibers, J. A. *Can. J. Chem.* **1995**, *73*, 1148.
(24) Martin, T. M.; Wood, P. T.; Kolis, J. W. *Inorg. Chem.* **1994**, *33*, 1587.
(25) Martin, T. M.; Schimek, G. L.; Pennington, W. T.; Kolis, J. W. *J. Chem. Soc., Dalton Trans.* **1995**, 501.
(26) Rudolph, R. W.; Wilson, W. L.; Taylor, R. C. *J. Am. Chem. Soc.* **1981**, *103*, 2480. The $\delta(^{125}Te)$ value reported for the $SnTe_4^{4-}$ anion in en solution in this reference is incorrect. Approximate ^{119}Sn and ^{125}Te chemical shifts were subsequently reported by Haushalter and co-workers,[27] and accurate values were later reported by Schrobilgen and co-workers.[28]
(27) Huffman, J. C.; Haushalter, J. P.; Umarji, A. M.; Shenoy, G. K.; Haushalter, R. C. *Inorg. Chem.* **1984**, *23*, 2312.
(28) Burns, R. C.; Devereux, L. A.; Granger, P.; Schrobilgen, G. J. *Inorg. Chem.* **1985**, *24*, 2615.
(29) Klepp, K. O. *Z. Naturforsch.* **1992**, *B47*, 411.

S0020-1669(95)00917-7 CCC: $12.00

lography; however, the monomeric $SnCh_3^{2-}$ (Ch = Se, Te) anions have not yet been isolated as salts but dimerize in the solid state to form $Sn_2Ch_6^{4-}$ anions.[27,31−36] Interestingly, the solution structures of the dimeric $Sn_2Ch_6^{4-}$ anions have never been reported. Moreover, several tin(IV) chalcogenide anions that are dinuclear in tin or have higher tin nuclearities have also been synthesized and characterized by X-ray crystallography as structural units in Zintl phases[37] (e.g., $Sn_2S_7^{6-}$,[38] $[Sn_2Se_5^{2-}]_\infty$,[39,40] $Sn_2Se_7^{6-}$,[41,42] $Sn_2Te_6^{6-}$,[43] $Sn_3Se_8^{4-}$,[44] $[Sn_3Se_7^{2-}]_\infty^2$ [45]) or as discrete units in Zintl salts (e.g., $Sn_4Se_{10}^{4-}$;[46] other examples are discussed in detail under **Results and Discussion**). Of the higher nuclearity tin(IV) species, only the $Sn_4Se_{10}^{4-}$ anion has been structurally characterized in solution by multi-NMR spectroscopy. Nuclear magnetic resonance spectroscopy of the spin $^1/_2$ nuclei ^{77}Se, ^{117,119}Sn, and ^{125}Te is particularly well suited for the solution characterization of tin(IV) chalcogenide anions and can provide additional valuable structural information based upon homo- and heteronuclear spin−spin couplings as well as aid in investigating the parameters which lead to condensation in solution.

Our synthetic strategy leading to the preparation of classically-bonded Zintl anions in solution has usually involved preparing and extracting ternary MXCh alloys (M = Na, K; X = Sn, Pb, Tl; Ch = S, Se, Te) in a basic, nonaqueous medium such as en or liquid NH_3 and in the presence of a stoichiometric excess of the macrobicyclic ligand 2,2,2-crypt, which serves to minimize ion-pairing by acting as a sequestering agent for M^+. Under conditions involving minimum ion-pairing, solutions arising from extraction of the alloys $KSnCh_2$ (Ch = Se, Te) in en were shown by multi-NMR spectroscopy to contain only the monomeric $SnCh_3^{2-}$ anions.[28] It was therefore of interest to investigate, through the use of solution NMR spectroscopy, the effect of varying amounts of unsequestered M^+ on the extent of condensation of the monomeric $SnCh_3^{2-}$ anions. Although the crystal structures of the $SnCh_3^{2-}$ anions remain uncharacterized, the X-ray crystal structure of the hydroxide derivative of the $SnTe_3^{2-}$ anion, $HOSnTe_3^{3-}$, is reported in this work. The Raman spectra of the $Sn_2Ch_6^{4-}$ (Ch = Se, Te) anions are also reported and are interpreted in light of their crystal structures.

Results and Discussion

(I) Synthesis of the $Sn_2Ch_6^{4-}$ and $Sn_2Ch_7^{4-}$ (Ch = Se, Te) Anions and Structural Characterization by ^{77}Se, ^{119}Sn, and ^{125}Te NMR Spectroscopy. The experimental approach involved the synthesis of the ternary alloys $KSn_{0.67}Se_{1.93}$, $KSn_{0.63}Te_{1.70}$, and $NaSn_{0.43}Te$ by fusion of the elements followed by extraction of the powdered alloys in en or liquid NH_3 in the absence (Te) or presence (Se) of nonstoichiometric amounts of 2,2,2-crypt with respect to M^+ (M = Na, K), where M^+:2,2,2-crypt = 1.00:0.42.

The $Sn_2Ch_6^{4-}$ and $Sn_2Ch_7^{4-}$ (Ch = Se, Te) anions present in solutions containing K^+ were identified by natural abundance ^{77}Se, ^{119}Sn, and ^{125}Te NMR spectroscopy. The experimental ^{77}Se, ^{119}Sn, and ^{125}Te NMR spectra and the simulated ^{119}Sn NMR spectra are depicted in Figures 1−4. The chemical shifts and spin−spin coupling constants of the new ditin anions as well as those of the previously characterized $SnCh_3^{2-}$ and $SnCh_4^{4-}$ anions[28] are listed in Table 1 together with the observed and calculated satellite/central peak (I_S/I_C) intensity ratios[21] of the Se, Te, and Sn environments of the anions. The number of observed environments, the satellite doublet spacings corresponding to $^1J(^{119}Sn-^{77}Se)$, $^1J(^{119}Sn-^{125}Te)$, and $^2J(^{119}Sn-^{117}Sn)$, and the I_S/I_C ratios are consistent with dimeric $SnCh_3^{2-}$ structures, $Sn_2Ch_6^{4-}$, and $Sn_2Ch_7^{4-}$ anion structures.

The ^{119}Sn and ^{77}Se NMR spectra of the yellow solutions obtained by extracting $KSn_{0.67}Se_{1.93}$ in en and liquid NH_3 in the presence of a nonstoichiometric amount of 2,2,2-crypt were recorded at 0 and −50 °C and showed several new signals (Figures 1 and 3). Although satellites were resolved in the ^{119}Sn NMR spectrum at both temperatures, the ^{119}Sn NMR resonances at 0 °C were broad and the ^{77}Se spectrum obtained at −50 °C contained a number of overlapping peaks which precluded accurate satellite assignments and I_S/I_C determinations. Consequently, subsequent discussion of the NMR parameters refers to those obtained at −50 (^{119}Sn) and 0 °C (^{77}Se), although Table 1 lists the parameters obtained at both temperatures. Resonances observed in the ^{119}Sn NMR spectrum at −491.6 (57 %) and −328.4 ppm (15 %) were assigned to the $Sn_2Se_6^{4-}$ and $Sn_2Se_7^{4-}$ anions, respectively, and are discussed under their respective subheadings (*vide infra*). Resonances observed at −299.5 (1%) and at −350.1 (27%) ppm in the ^{119}Sn NMR spectrum were assigned to the known $SnSe_3^{2-}$ anion[28] and to the adamantanoid $Sn_4Se_{10}^{4-}$ anion,[46] which was recently characterized by ^{77}Se and ^{119}Sn NMR spectroscopy, X-ray crystallography, and Raman spectroscopy. Selenium resonances were observed at 295.1 and 37.6 ppm for the $Sn_2Se_6^{4-}$ anion; 116.8, −30.2, and −58.1 ppm for the $Sn_2Se_7^{4-}$ anion; 65.0 and 22.2 ppm for the $Sn_4Se_{10}^{4-}$ anion; and −91.0 ppm for the $SnSe_3^{2-}$ anion.

The ^{119}Sn and ^{125}Te NMR spectra of the dark red solution obtained upon extraction of $KSn_{0.63}Te_{1.70}$ in liquid NH_3 in the absence[47] of 2,2,2-crypt were recorded at −70 °C (Figures 2 and 4). The signal at −1230.1 ppm (32%)[48] in the ^{119}Sn NMR spectrum was assigned to the previously characterized trigonal-planar $SnTe_3^{2-}$ anion.[28] The ^{125}Te and the ^{123}Te satellites were well resolved [$^1J(^{119}Sn-^{125}Te)$ = 4487 Hz; $^1J(^{119}Sn-^{123}Te)$ = 3726 Hz], and the ratio $^1J(^{119}Sn-^{125}Te)/^1J(^{119}Sn-^{123}Te) = 1.204$ (hereafter referred to as R_J) is in excellent agreement with the ratio of the gyromagnetic ratios $\gamma(^{125}Te)/\gamma(^{123}Te) = 1.206$ (hereafter referred to as R_γ). In addition, the triplet subspectrum arising from coupling of the ^{119}Sn nucleus to two spin-active ^{125}Te nuclei was observed. Three additional resonances were

(30) Eisenmann, B.; Schäfer, H.; Schrod, H. *Z. Naturforsch.* **1983**, *B38*, 921.
(31) Krebs, B.; Uhlen, H. *Z. Anorg. Allg. Chem.* **1987**, *549*, 35.
(32) Eisenmann, B.; Hansa, J. *Z. Kristallogr.* **1983**, *203*, 299.
(33) Sheldrick, W. S.; Schaaf, B. *Z. Anorg. Allg. Chem.* **1994**, *620*, 1041.
(34) Sheldrick, W. S.; Braunbeck, H.-G. *Z. Naturforsch.* **1989**, *B44*, 851.
(35) Sheldrick. W. S.; Braunbeck, H. G. *Z. Anorg. Allg. Chem.* **1993**, *619*, 1300.
(36) Ansari, M. A.; Bollinger, J. C.; Ibers, J. A. *Inorg. Chem.* **1993**, *32*, 231.
(37) For example, the $[SnSe_3^{2-}]_\infty$ anion in the Zintl phases Na_2SnSe_3-I (Eisenmann, B.; Hansa, J. *Z. Kristallogr.* **1993**, *203*, 291) and Na_2SnSe_3-II (Eisenmann, B.; Hansa, J. *Z. Kristallogr.* **1993**, *203*, 293).
(38) Krebs, B.; Schiwy, W. *Z. Anorg. Allg. Chem.* **1973**, *398*, 63.
(39) Sheldrick, W. W.; Braunbeck, H.-G. *Z. Naturforsch.* **1992**, *B47*, 151.
(40) Klepp, K. O. *Z. Naturforsch.* **1992**, *B47*, 197.
(41) Eisenmann, B.; Hansa, J. *Z. Kristallogr.* **1993**, *203*, 297.
(42) Eisenmann, B.; Hansa, J. *Z. Kristallogr.* **1993**, *203*, 303.
(43) Dittmar, G. *Z. Anorg. Allg. Chem.* **1978**, *453*, 68.
(44) Sheldrick, W. S. *Z. Naturforsch.* **1988**, *B43*, 249.
(45) Sheldrick, W. S.; Braunbeck, H.-G. *Z. Naturforsch.* **1990**, *B45*, 1643.
(46) Campbell, J.; DiCiommo, D. P.; Mercier, H. P. A.; Pirani, A. M.; Schrobilgen, G. J.; Willuhn, M. *Inorg. Chem.* **1995**, *34*, 6265.

(47) The ^{119}Sn and ^{125}Te NMR spectra of the liquid NH_3 extract of the alloy $KSn_{0.63}Te_{1.70}$ containing a K^+:2,2,2-crypt stoichiometry of 1.00:0.44 could not be recorded at −70 °C, as the sample gave rise to a large amount of crystalline material at this temperature. At temperatures above −70 °C, severe broadening of the NMR resonances prevented accurate satellite assignments and I_S/I_C determinations.

(48) Because of the large dynamic chemical shift range of ^{119}Sn, accurate integrations of the resonances corresponding to $SnTe_3^{2-}$, $Sn_2Te_6^{4-}$, and $Sn_2Te_7^{4-}$ could only be obtained by recording the ^{119}Sn NMR spectrum at lower field (7.0463 T).

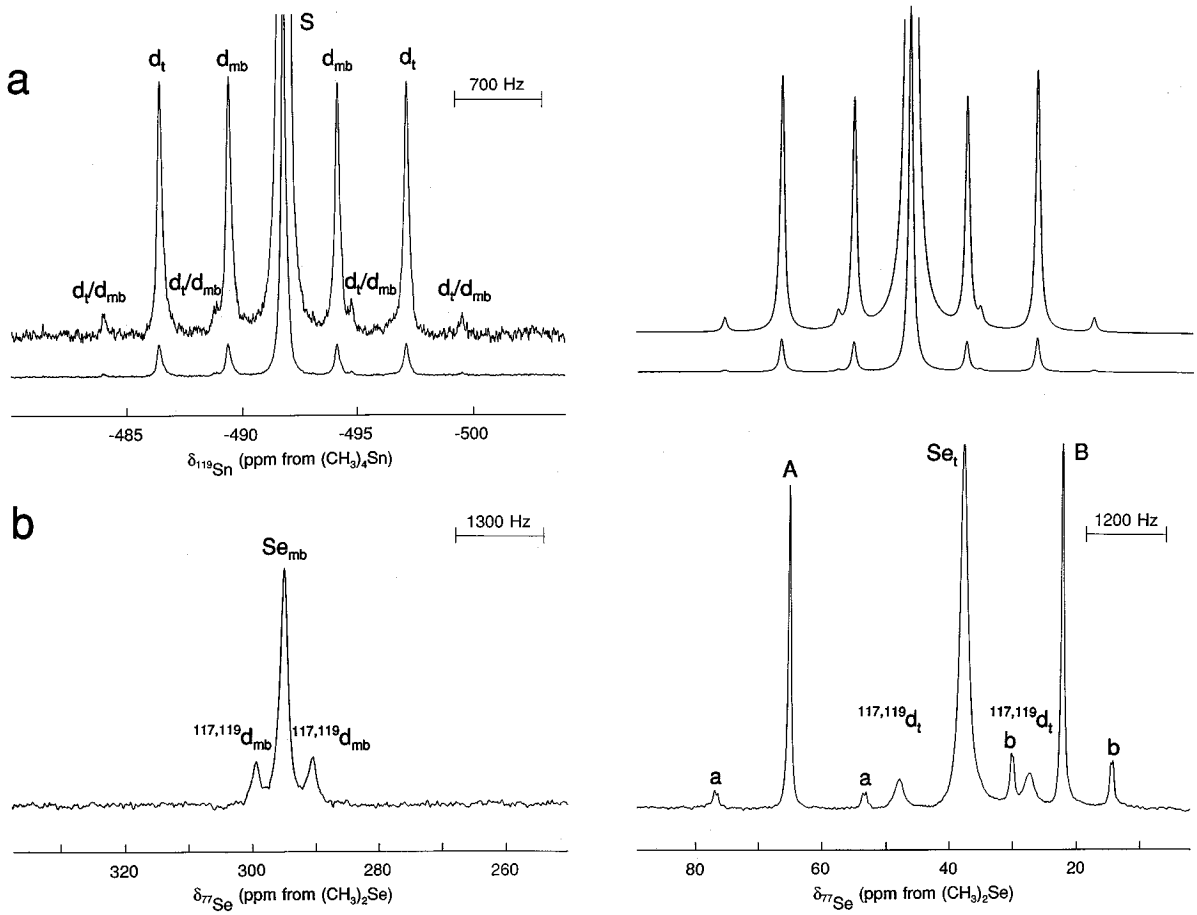

Figure 1. NMR spectra of the $Sn_2Se_6^{4-}$ anion: (a) ^{119}Sn (186.504 MHz) recorded in liquid NH_3 at −50 °C and simulated spectrum (right-hand trace); (b) ^{77}Se (95.383 MHz) recorded in en at 0 °C. The symbols used to label the peaks in the ^{119}Sn NMR spectrum are defined in Table 2 and in the text. In both the ^{119}Sn and ^{77}Se NMR spectra, $^{117,119}d_{mb}$ and $^{117,119}d_t$ denote satellite doublets arising from $^1J(^{117,119}Sn-^{77}Se_{mb})$ and $^1J(^{117,119}Sn-^{77}Se_t)$, respectively. The symbols in the ^{77}Se NMR spectrum, Se_{mb} and Se_t, denote the monoseleno-bridging and terminal selenium environments, respectively, and (A) and (B) correspond to the terminal and bridging selenium environments of the $Sn_4Se_{10}^{4-}$ anion.[46]

observed in the ^{119}Sn NMR spectrum at lower frequencies relative to the $SnTe_3^{2-}$ anion (−1675.0 ppm, 34%; −1344.9 ppm, 28%; −1267.5 ppm, 6%) which did not correspond to known species. The resonances at −1675.0 and −1344.9 ppm were assigned to the $Sn_2Te_6^{4-}$ and $Sn_2Te_7^{4-}$ anions, respectively, and are discussed under their respective subheadings (*vide infra*). The weak signal at −1267.5 ppm could not be assigned, as ^{125}Te satellites were not observed. The ^{125}Te resonance of the $SnTe_3^{2-}$ anion was observed at −476.8 ppm, and the ^{125}Te signals associated with the ditin anions were observed at 458.3 and −89.3 ppm ($Sn_2Te_6^{4-}$) and at −323.5, −124.8, and −95.1 ppm ($Sn_2Te_7^{4-}$). The remaining weak resonances at −30.2, −137.9, and −161.2 ppm could not be assigned because $^{117,119}Sn$ satellites were not observed.

The ^{119}Sn and ^{125}Te NMR spectra (−70 °C) of the intense red liquid NH_3 extract of the $NaSn_{0.43}Te$ alloy in the absence of 2,2,2-crypt gave rise to two and four signals, respectively. The most intense signal in the ^{119}Sn NMR spectrum (−1749.8 ppm, 90%) was assigned to the previously characterized tetrahedral $SnTe_4^{4-}$ anion.[28] The weaker signal (−1155.2 ppm, 10%) consisted of a broad singlet flanked by a pair of ^{125}Te satellites [$^1J(^{119}Sn-^{125}Te) = 4376$ Hz] and was assigned to the $SnTe_3^{2-}$ anion (see **$SnCh_3^{2-}$ (Ch = Se, Te) Condensation Processes**). The ^{125}Te resonances of the $SnTe_4^{4-}$ [$^1J(^{125}Te-^{119}Sn) = 2960$ Hz and $^1J(^{125}Te-^{117}Sn) = 2826$ Hz; $R_J = 1.045$ and $R_\gamma = 1.046$)] and $SnTe_3^{2-}$ anions were observed at −281.8 and −506.7 ppm, respectively. The remaining weak signals in the ^{125}Te NMR spectrum (−370.4 and −591.9 ppm) could not be assigned.

Solution Structures of the $Sn_2Se_6^{4-}$ and $Sn_2Te_6^{4-}$ Anions. The ^{119}Sn NMR spectrum of the $Sn_2Se_6^{4-}$ anion (Figure 1) consisted of a singlet (−491.6 ppm) flanked by two pairs of ^{77}Se satellites (d_{mb}, 888 Hz; d_t, 2005 Hz) in a 1.0:1.0 peak area ratio, indicating coupling to two chemically inequivalent selenium environments. In addition, four weaker ^{77}Se satellites were observed in the ^{119}Sn NMR spectrum (d_t/d_{mb} in Figure 1), and their assignments are discussed below. The two associated selenium environments were observed in the ^{77}Se NMR spectrum at 295.1 and 37.6 ppm with a relative peak area ratio of 2.0:4.2. The I_S/I_C ratios of the accompanying tin satellites (Table 1) indicated that the two selenium environments were coupled to two and one tin atoms, respectively. These findings are consistent with the solid state D_{2h} point symmetry of the $Sn_2Se_6^{4-}$ anion (see **X-ray Crystal Structures**). The ^{77}Se peaks at 295.1 and 37.6 ppm were assigned to the monoseleno-bridge, Se_{mb}, and terminal, Se_t, selenium environments of the anion, respectively. The smaller coupling was consequently assigned to $^1J(^{119}Sn-^{77}Se_{mb})$ and the larger coupling to $^1J(^{119}Sn-^{77}Se_t)$. The coexistence of the $SnSe_3^{2-}$ and $Sn_2Se_6^{4-}$ anions implies that both anions are in equilibrium (eq 1) and that the

$$2SnSe_3^{2-} \rightleftharpoons Sn_2Se_6^{4-} \quad (1)$$

equilibrium is shifted toward the dimer under conditions allowing ion-pair formation (see **$SnCh_3^{2-}$ (Ch = Se, Te) Condensation Processes**). This is noteworthy because the $SnSe_3^{2-}$ anion is known as the major species in K/Sn/Se alloy extracts containing stoichiometric excesses of 2,2,2-crypt with respect to K^+.[28]

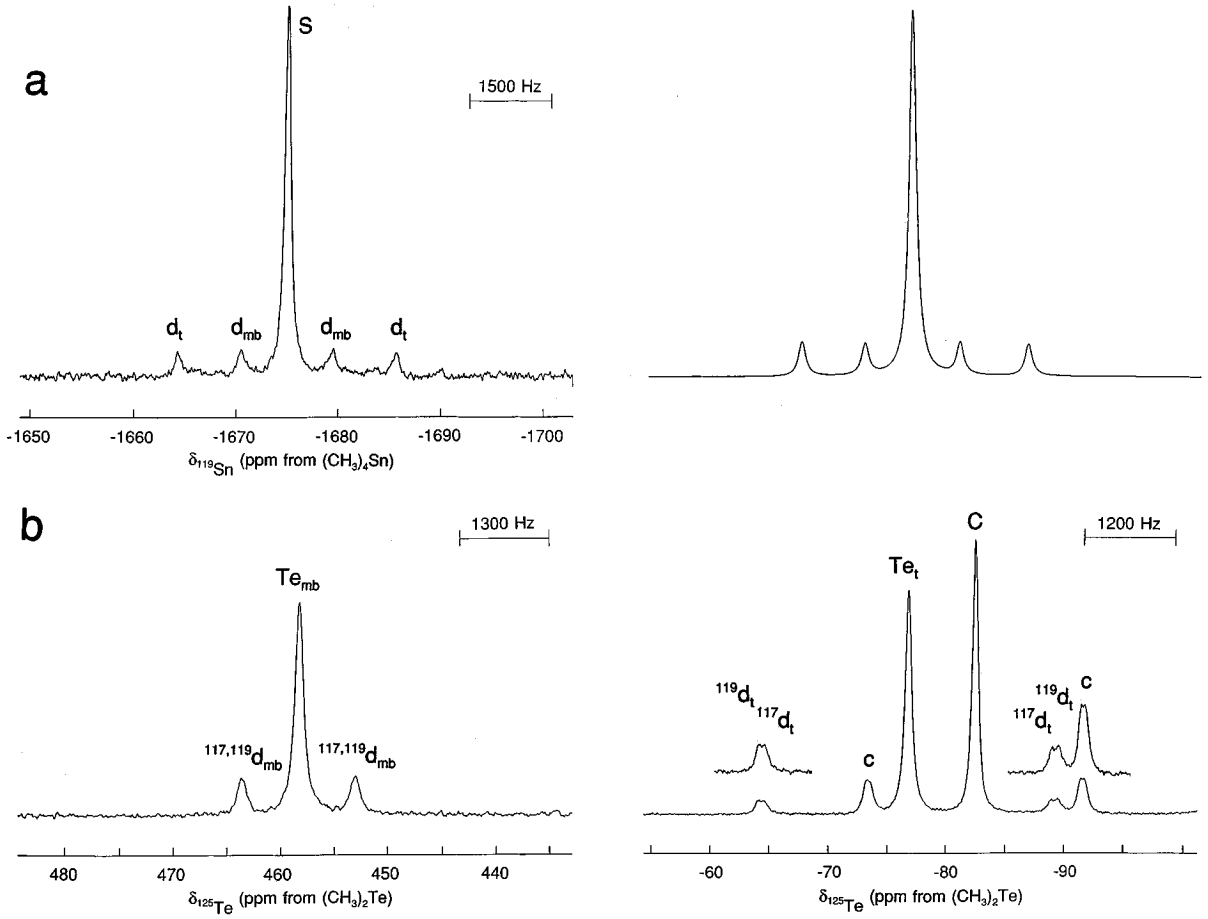

Figure 2. NMR spectra of the $Sn_2Te_6^{4-}$ anion recorded in liquid NH_3 at −70 °C: (a) ^{119}Sn (186.504 MHz) and simulated spectrum (right-hand trace); (b) ^{125}Te (157.794 MHz). The symbols used to label the peaks in the ^{119}Sn NMR spectrum are defined in Table 2 and in the text. In both the ^{119}Sn and ^{125}Te NMR spectra, $^{117,119}d_{mb}$ and $^{117,119}d_t$ denote satellite doublets arising from $^1J(^{117,119}Sn-^{125}Te_{mb})$ and $^1J(^{117,119}Sn-^{125}Te_t)$, respectively. The symbols in the ^{125}Te NMR spectrum, Te_{mb} and Te_t, denote the monotelluro-bridging and terminal tellurium environments, respectively, and (C) corresponds to the terminal tellurium environment of the $Sn_2Te_7^{4-}$ anion.

The ^{119}Sn and ^{125}Te NMR spectra of the $Sn_2Te_6^{4-}$ anion (Figure 2) were similar to those observed for the $Sn_2Se_6^{4-}$ anion. The ^{119}Sn NMR spectrum consisted of a singlet (−1675.0 ppm) flanked by two sets of satellites arising from $^1J(^{119}Sn-^{125}Te)$ couplings (d_{mb}, 1683 Hz, and d_t, 3998 Hz; peak area ratio, 1.1:1.0). The counterparts to the four weak satellites observed in the ^{119}Sn NMR spectrum of $Sn_2Se_6^{4-}$ were not observed in the ^{119}Sn spectrum of $Sn_2Te_6^{4-}$ because the signals were broadened. The ^{125}Te resonances of $Sn_2Te_6^{4-}$ were observed at 458.3 (Te_{mb}) and at −89.3 ppm (Te_t) with a relative peak area ratio of 2.0:4.3.

Solution Structures of the $Sn_2Se_7^{4-}$ and $Sn_2Te_7^{4-}$ Anions. The ^{119}Sn NMR spectrum of $Sn_2Se_7^{4-}$ (Figure 3) consisted of a singlet (−328.4 ppm) flanked by three sets of ^{77}Se satellites (d_{db}, 1134 Hz; d_{mb}, 1324 Hz; d_t, 2037 Hz) having relative peak areas of 1.0:1.2:2.1, which are consistent with coupling to three inequivalent selenium environments. Satellites corresponding to a $^2J(^{119}Sn-^{117}Sn)$ coupling of 302 Hz were also observed in the ^{119}Sn NMR spectrum; this coupling is similar to that observed for $Sn_4Se_{10}^{4-}$ (342 Hz).[46] Comparable $^2J(^{119}Sn-^{117}Sn)$ values of 205, 235, and 263 Hz have been observed for the solution structures of the dimethyltin(IV) chalcogenides $[(CH_3)_2SnCh]_3$ (Ch = S, Se, Te), respectively.[49] The ^{77}Se signals corresponding to the three Se environments of $Sn_2Se_7^{4-}$ were observed at 116.8, −30.2, and −58.1 ppm, respectively (relative peak areas, 1.9:1.0:4.4). The I_S/I_C ratios of the accompanying ^{119}Sn satellites indicated that the Se environments were bonded to one, two, and one Sn atoms, respectively. These findings are consistent with a ditin selenide anion, $Sn_2Se_7^{4-}$ (structure **I**). Although the crystal structure of the $Sn_2Se_7^{4-}$ anion is

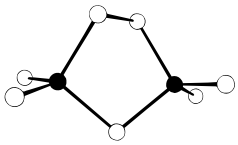

I

unknown, the telluride analog has been characterized by X-ray crystallography in $Cs_4Sn_2Te_7$.[50] The ^{77}Se peaks at 116.8, −30.2, and −58.1 ppm were assigned to Se_{db} (db, diseleno-bridge), Se_{mb}, and Se_t, respectively. The smallest coupling was consequently assigned to $^1J(^{119}Sn-^{77}Se_{db})$, the intermediate coupling to $^1J(^{119}Sn-^{77}Se_{mb})$, and the largest coupling to $^1J(^{119}Sn-^{77}Se_t)$.

By analogy with that of the $Sn_2Se_7^{4-}$ anion, the ^{119}Sn NMR spectrum of the $Sn_2Te_7^{4-}$ anion (Figure 4) consisted of a singlet (−1344.9 ppm) flanked by three pairs of ^{125}Te satellites (d_{db}, 2319 Hz, d_{mb}, 2902 Hz, and d_t, 4023 Hz, with relative peak

(49) Gay, I. D.; Jones, C. H. W.; Sharma, R. D. *J. Magn. Reson.* **1989**, *84*, 501.

(50) Brinkmann, C.; Eisenmann, B.; Schäfer, H. *Mater. Res. Bull.* **1985**, *20*, 299.

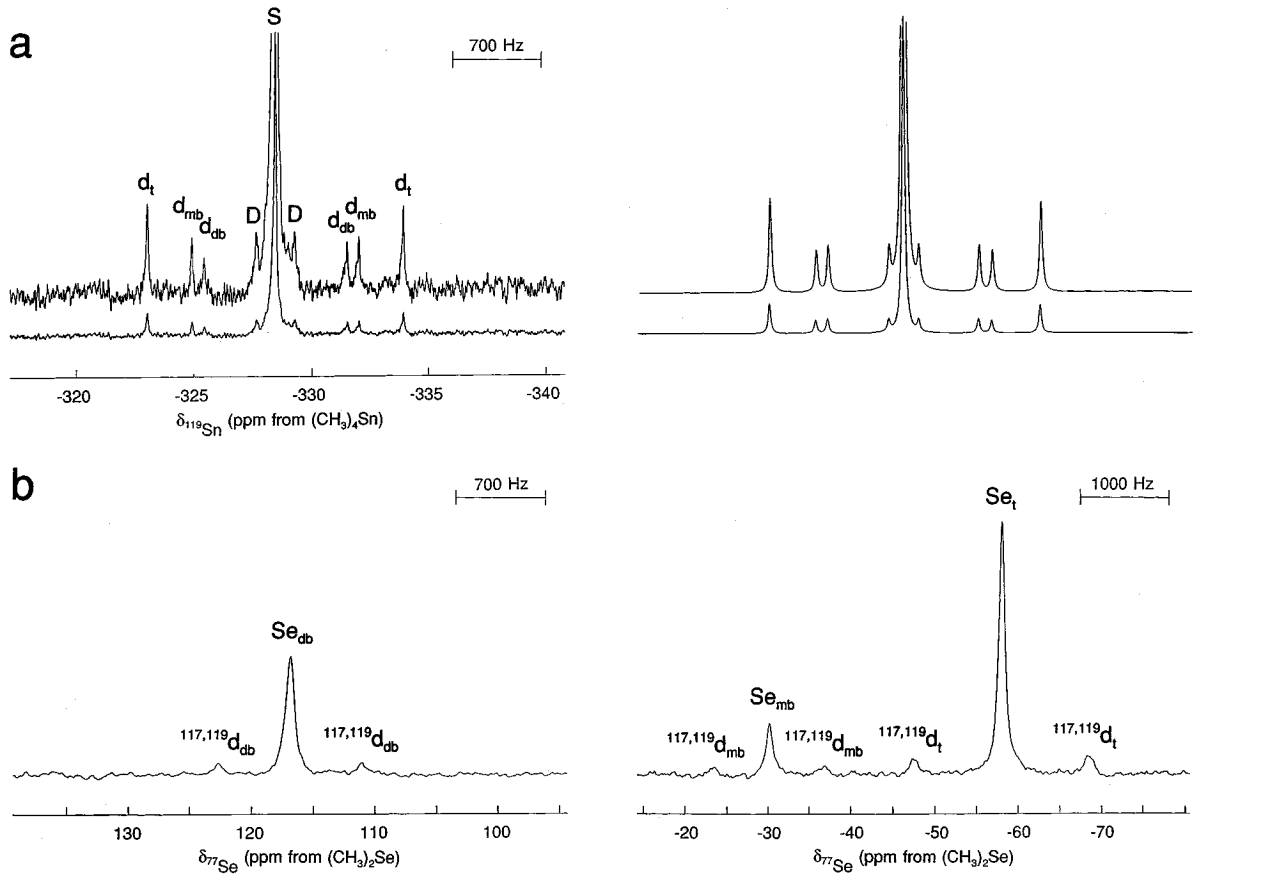

Figure 3. NMR spectra of the $Sn_2Se_7^{4-}$ anion: (a) ^{119}Sn (186.504 MHz) recorded in liquid NH_3 at −50 °C and simulated spectrum (right-hand trace); (b) ^{77}Se (95.383 MHz) recorded in en at 0 °C. The symbols used to label the peaks in the ^{119}Sn NMR spectrum are defined in Table 2 and in the text. In both the ^{119}Sn and ^{77}Se NMR spectra, $^{117,119}d_{db}$, $^{117,119}d_{mb}$, and $^{117,119}d_t$ denote satellite doublets arising from $^1J(^{117,119}Sn-^{77}Se_{db})$, $^1J(^{117,119}Sn-^{77}Se_{mb})$, and $^1J(^{117,119}Sn-^{77}Se_t)$, respectively. The symbols in the ^{77}Se NMR spectrum, Se_{db}, Se_{mb}, and Se_t, denote the diseleno-bridging, monoseleno-bridging, and terminal selenium environments, respectively.

areas of 1.0:1.1:1.8). The ^{125}Te NMR spectrum consisted of three environments at −124.8 (Te_{db}), −95.1 (Te_{mb}), and −323.5 ppm (Te_t) with relative peak areas of 2.2:1.0:3.9.

The ^{119}Sn NMR spectra of the $Sn_2Ch_6^{4-}$ and $Sn_2Ch_7^{4-}$ anions were simulated using the natural abundances of the spin $^1/_2$ nuclei ^{77}Se, ^{117}Sn, ^{119}Sn, and ^{125}Te;[51] the values of the observed coupling constants (Table 1); and the total line intensities and multiplicities of the most abundant isotopomers (Tables 2 and 3) contributing significant first-order subspectra to the experimental ^{119}Sn NMR spectra. The resulting simulations (Figures 1−4) are in excellent agreement with the experimental spectra and account for all of the observed satellite peaks. A singlet (S) is observed for the isotopomers in which no *Ch (*Ch = ^{77}Se or ^{125}Te) atoms are directly bonded to spin-active Sn atoms, namely, $^{119}Sn_xSn_{2-x}{*}Ch_zCh_{y-z}^{4-}$ [$x = 1, 2$; $y = 6$ ($Sn_2Ch_6^{4-}$), 7 ($Sn_2Ch_7^{4-}$); $z = 0-2$]. When one *Ch atom is in a terminal or bridging position directly bonded to a ^{119}Sn atom, a doublet (d_t, d_{mb}, or d_{db}) results which is symmetrically disposed about the central singlet (S) at a spacing corresponding to $^1J(^{119}Sn-{*}Ch_t)$, $^1J(^{119}Sn-{*}Ch_{mb})$, or $^1J(^{119}Sn-{*}Ch_{db})$, respectively. The $^{119}Sn^{117}Sn{*}Ch_zCh_{y-z}^{4-}$ isotopomers give rise to a DOUBLET (D) resulting from $^2J(^{119}Sn-^{117}Sn)$ coupling when no *Ch atoms are directly bonded to ^{119}Sn atoms. The presence of a *Ch atom in a terminal (D/d_t), monochalcogeno (D/d_{mb})- or dichalcogeno (D/d_{db})-bridging position directly bonded to a ^{119}Sn atom produces a DOUBLET-of-doublets whose transitions are symmetrically disposed about the doublets d_t, d_{mb}, or d_{db}, respectively. The $^{119}Sn_xSn_{2-x}{*}Ch_2Ch_y^{4-}$ [$y = 4$ ($Sn_2Ch_6^{4-}$), 5 ($Sn_2Ch_7^{4-}$)] isotopomers result in a doublet-of-doublets (d_t/d_{mb}, d_t/d_{db}, or d_{mb}/d_{db}) when the *Ch atoms are appropriately positioned and directly bonded to at least one ^{119}Sn atom, e.g., one *Ch atom in a terminal position and one in a monochalcogeno-bridging position directly bonded to a ^{119}Sn atom produces a d_t/d_{mb} doublet-of-doublets. The transitions of the doublet-of-doublets are observed symmetrically disposed about the central singlet.

Coupling Constants (J) and Reduced Coupling Constants (K and K_{RC}). In general, spin−spin couplings between nuclei of heavy atoms connected by single rather than multiple bonds are dominated by the Fermi contact mechanism.[52] In terms of the formalism developed by Pople and Santry,[53] the Fermi contact mechanism is given by eq 2, where all symbols have

$$J_{AB} = 16\frac{\pi^2}{9h}\left(\frac{g\beta h}{2\pi}\right)^2 \gamma_A\gamma_B|\psi_{ns,A}(0)|^2|\psi_{ns,B}(0)|^2\Pi_{AB} \quad (2)$$

their usual meanings and/or values; γ_A and γ_B represent the gyromagnetic ratios of the coupled nuclei; $|\psi_{ns,A}(0)|^2$ and $|\psi_{ns,B}(0)|^2$ are the s-electron densities for the valence ns orbitals at nuclei A and B; and Π_{AB} is the mutual polarizability of the ns orbitals on A and B. In order to make comparisons between

(51) Mason, J. In *Multinuclear NMR*; Mason, J., Ed.; Plenum Press: New York, 1987; Appendix, pp 626−627.

(52) Jameson, C. J. In *Multinuclear NMR*; Mason, J., Ed.; Plenum Press: New York, 1987; Chapter 4, p 89.

(53) Pople, J. A.; Santry, D. P. *Mol. Phys.* **1964**, *8*, 1.

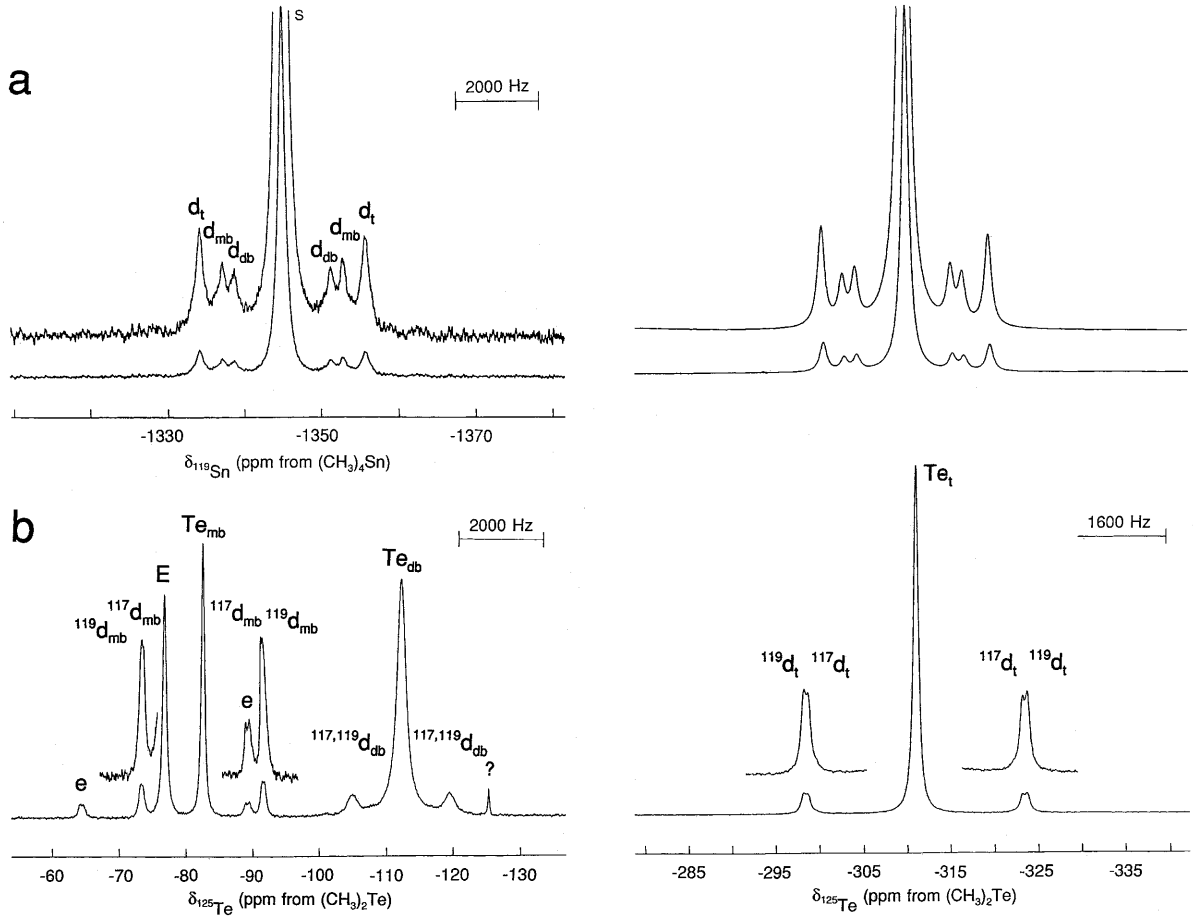

Figure 4. NMR spectra of the $Sn_2Te_6^{4-}$ anion recorded in liquid NH_3 at −70 °C: (a) ^{119}Sn (186.504 MHz) and simulated spectrum (right-hand trace); (b) ^{125}Te (157.794 MHz). The symbols used to label the peaks in the ^{119}Sn NMR spectrum are defined in Table 2 and in the text. In both the ^{119}Sn and ^{125}Te NMR spectra, $^{117,119}d_{mb}$, $^{117,119}d_{db}$, and $^{117,119}d_t$ denote satellite doublets arising from $^1J(^{117,119}Sn-^{125}Te_{mb})$, $^1J(^{117,119}Sn-^{125}Te_{db})$, and $^1J(^{117,119}Sn-^{125}Te_t)$, respectively. The symbols in the ^{125}Te NMR spectrum, Te_{mb}, Te_{db}, and Te_t, denote the monotelluro-bridging, ditelluro-bridging, and terminal tellurium atoms, respectively. (E) corresponds to the terminal tellurium environments of the $Sn_2Te_6^{4-}$ anion and (?) indicates an unassigned resonance.

couplings in a series of structurally related species having different spin-coupled nuclei, it is necessary to remove the nuclear dependence on J_{AB}. If the Fermi contact mechanism is assumed to be the dominant contributor to J_{AB}, then the reduced coupling constant, K_{AB},[53] as defined by eq 3, provides

$$K_{AB} = \frac{4\pi^2}{h\gamma_A\gamma_B} J_{AB} \qquad (3)$$

a better representation of electronic environments in molecules. Pyykkö and Wiesenfeld[54] have shown that relativistic effects on the Fermi contact term (s-electron density) dominate K_{AB} for heavy main-group elements. Previous work on spin−spin couplings in classically-bonded trigonal-planar MCh_3^{n-},[28] tetrahedral $SnCh_4^{4-}$,[28] and trigonal-bipyramidal $M_2Ch_3^{n-}$ [21,55] anions (M = Sn, Pb, or Tl; Ch = S, Se, and/or Te; n = 2 or 3) as well as in $HgCh_2^{2-}$ and $CdCh_2^{2-}$ (Ch = Se, Te)[28] has illustrated a method for factoring out the relativistic effects on $|\psi_{ns}(0)|^2$. The correction for a given element is determined by applying the ratio $|\psi_{ns}(0)|^2_{rel}/|\psi_{ns}(0)|^2_{nonrel}$. Values for relativistic and nonrelativistic s-electron densities taken from the work of Pyykkö and Wiesenfeld[54] give the following ratios: Sn, 1.425; Se, 1.155; Te, 1.439. The reduced coupling constants, ^1K(Sn−Ch), and the relativistically corrected reduced coupling constants, $^1K(Sn-Ch)_{RC}$, for the $Sn_2Ch_6^{4-}$ and $Sn_2Ch_7^{4-}$ anions and those for the previously characterized $SnCh_3^{2-}$ and $SnCh_4^{4-}$ anions are listed in Table 4.

The large $^1K(Sn-Ch)_{RC}$ values for the $Sn_2Ch_6^{4-}$ and $Sn_2Ch_7^{4-}$ anions indicate a significant s-component to the bonding and contrast with the smaller values determined for the essentially pure p-bonded trigonal-bipyramidal $M_2Ch_3^{2-}$ cages (M = Sn,[55] Pb[21]). The magnitudes of $^1K(Sn-Ch)_{RC}$ for the $Sn_2Ch_6^{4-}$ and $Sn_2Ch_7^{4-}$ anions can be correlated with the degree of hybridization at the Sn atoms, and hence the degree of s-character in the Sn−Ch bonds, by comparison with analogous $^1K_{RC}$ values for the formally sp^2- and sp^3-hybridized $SnCh_3^{2-}$ and $SnCh_4^{4-}$ anions, respectively. The $^1K(Sn-Ch_t)_{RC}$ values for $Sn_2Ch_6^{4-}$ and $Sn_2Ch_7^{4-}$ are similar to, but smaller than, those observed for the $SnCh_3^{2-}$ anions. The Sn hybrid orbitals involved in bonding to Ch_t can therefore be described as having less s-character than sp^2-hybridized $SnCh_3^{2-}$ orbitals. The larger $^1K(Sn-Ch)_{RC}$ values for Ch_t when compared to those for Ch_{mb} and Ch_{db} are consistent with higher relative bond orders in the Sn−Ch_t bonds than in the Sn−Ch_{mb} and Sn−Ch_{db} bonds. This is reflected in the shorter Sn−Ch_t bond distances [average: Se, 2.460(4) Å; Te, 2.669(4) Å] and larger Sn−Ch_{mb} bond distances [average: Se, 2.592(4) Å; Te, 2.817(4) Å] observed for the $Sn_2Ch_6^{4-}$ anions in compounds **1**−**3** (see **X-ray Crystal Structures**). The differences in the magnitudes of $^1K(Sn-Te)_{RC}$ determined for the $Sn_2Te_7^{4-}$ anion are also reflected in the Sn−Te_t [2.683(3) Å], Sn−Te_{mb} [2.808(2) Å], and Sn−Te_{db} [2.800(2)

(54) Pyykkö, P.; Wiesenfeld, L. *Mol. Phys.* **1981**, *43*, 557.
(55) Björgvinsson, M.; Mercier, H. P. A.; Mitchell, K. M.; Schrobilgen, G. J.; Strohe, G. *Inorg. Chem.* **1993**, *32*, 6046.

Table 1. Chemical Shifts, Spin−Spin Coupling Constants, and Satellite Intensities for the $SnCh_4^{4-}$, $Sn_2Ch_6^{4-}$, $Sn_2Ch_7^{4-}$, and $SnCh_3^{2-}$ (Ch = Se, Te) Anions

	chem shift, ppm[a]			spin−spin coupling constants *J*, Hz					$100 \times I_S/I_C$[b]		
anion	^{119}Sn	^{125}Te	^{77}Se	^{119}Sn−^{125}Te	^{117}Sn−^{125}Te	^{119}Sn−^{77}Se	^{117}Sn−^{77}Se	^{119}Sn−^{117}Sn	Sn	Te	Se
$SnTe_4^{4-}$	−1824[c]	−203		2851	2727						
	−1749.8[d]	−281.8		2960	2826				15.5 (16.8)	9.1 (9.6)	
$Sn_2Te_6^{4-}$	−1675.0[e]	−89.3 (t)		3998 (t)	3839 (t)				6.2 (8.5)	17.2 (19.2)	
		458.3 (mb)		1683 (mb)					6.9 (8.5)	7.2 (9.6)	
$Sn_2Te_7^{4-}$	−1344.9[e]	−323.5 (t)		4023 (t)	3946 (t)				7.1 (8.5)	6.2 (9.6)	
		−95.1 (mb)		2902 (mb)					5.1 (4.3)	13.8 (19.2)	
		−124.8 (db)		2319 (db)					4.6 (4.3)	10.3 (9.6)	
$SnTe_3^{2-}$ [f]	−1170[c]	−385		4535	4335						
	−1230.1[e]	−476.8		4487	4309						
	−1155.2[d]	−506.7		4376					12.3 (11.3)	7.9 (9.6)	
$SnSe_4^{4-}$	−476.6[c]		−61.9			1463	1398				
$Sn_2Se_6^{4-}$	−499[g]		37.6 (t)			2014 (t)					11.0 (9.6)
			295.1 (mb)			873 (mb)					21.4 (19.2)
	−491.6[h]		9.2 (t)			2005 (t)			7.2 (8.2)		
			266.4 (mb)			888 (mb)			7.6 (8.2)		
$Sn_2Se_7^{4-}$	−338[g]		−58.1 (t)			2045 (t)		268			20.1 (19.2)
			−30.2 (mb)			1306 (mb)					18.4 (19.2)
			116.8 (db)			1130 (db)					10.0 (9.6)
	−328.4[h]		−88.8 (t)			2037 (t)		302	7.4 (8.2)		
			−59.8 (mb)			1324 (mb)			3.8 (4.1)		
			106.4 (db)			1134 (db)			3.5 (4.1)		
$SnSe_3^{2-}$	−264.3[c]		−92.16[c]			2051					
	−299.5[h]		−91.0[g]								

[a] The symbols t, mb, and db denote the terminal chalcogen and monochalcogeno- and dichalcogeno-bridging environments. [b] Calculated values are given in parentheses. [c] Recorded in en solvent (24 °C) containing a stoichiometric excess of 2,2,2-crypt with respect to K^+.[28] [d][e] Recorded in NH_3 solvent (−70 °C) containing unsequestered Na^+ [K^+]. [f] $^1J(^{119}Sn-^{123}Te)$ = 3776 [3726] Hz in en [NH_3] solvent (24 [−70] °C) containing a stoichiometric excess[28] [absence] of 2,2,2-crypt with respect to K^+. [g][h] Recorded in en [NH_3] solvent (0 [−50] °C) containing a K^+:2,2,2-crypt ratio of 1.00:0.42.

Å] bond distances observed in $Cs_4Sn_2Te_7$.[50] The similarity between $^1K(Sn-Ch_{mb})_{RC}$ and $^1K(Sn-Ch)_{RC}$ for the $Sn_2Ch_7^{4-}$ and $SnCh_4^{4-}$ anions, respectively, suggests that the Sn(IV) orbitals involved in bonding to Ch_{mb} are essentially sp^3-hybridized. The smaller $^1K_{RC}$ values observed for Sn−Ch_{mb} and Sn−Ch_{db} in $Sn_2Ch_6^{4-}$ and $Sn_2Ch_7^{4-}$, respectively, indicate a substantial decrease in the s-character of the Sn hybrid orbitals. This is reflected in the average Ch_{mb}−Sn−Ch_{mb} bond angles [Se, 92.94(7)°; Te, 93.41(9)°] observed in the $Sn_2Ch_6^{4-}$ anions, which are considerably smaller than the ideal tetrahedral angle of 109.5° (see **X-ray Crystal Structures**).

Other than for $SnCh_3^{2-}$, $SnCh_4^{4-}$, and $Sn(Se_4)_3^{2-}$,[56] there is a lack of NMR data pertaining to classically-bonded Sn/Se or Sn/Te systems, and no scalar couplings have been reported for the $Sn(Se_4)_3^{2-}$ anion. However, the magnitudes of $^1J(^{119}Sn-Ch_{mb})$ for $Sn_2Ch_6^{4-}$ and $Sn_2Ch_7^{4-}$ are comparable with those determined for substituted tin−chalcogen cages in which the tin atom environment is approximately tetrahedral and that about the chalcogens is bent: $[(CH_3)_2SnSe]_3$, $^1J(^{119}Sn-^{77}Se_b)$ = 1219 Hz; $[(CH_3)_2SnTe]_3$; $^1J(^{119}Sn-^{125}Te_b)$ = 3103 Hz.[49] Other compounds containing tetrahedral tin environments include Sn(SePh)$_4$ [$^1J(^{119}Sn-^{77}Se)$ = 1584 Hz] and Sn(TePh)$_4$ [$^1J(^{119}Sn-^{125}Te)$ = 3379 Hz].[57]

Chemical Shifts. The ^{119}Sn chemical shifts of the $Sn_2Ch_6^{4-}$ (Se, −491.6 ppm; Te, −1675.0 ppm) and $Sn_2Ch_7^{4-}$ (Se, −328.4 ppm; Te, −1344.9 ppm) anions appeared in the Sn(IV) region and were accompanied by the ^{119}Sn NMR resonances of the $SnCh_3^{2-}$ (Se, −299.5 ppm; Te, −1230.1 ppm). Similar ^{119}Sn chemical shifts have also been reported for the $SnCh_4^{4-}$ anions, i.e., Se, −476.6 ppm, and Te, −1824 ppm.[28] As expected, on the basis of the electronegativity difference between Se and Te,[58] the Sn resonances for the Se anions were more deshielded than those for the Te analogs.

For both the $Sn_2Ch_6^{4-}$ and $Sn_2Ch_7^{4-}$ anions, the signals corresponding to the terminal chalcogen, Ch_t, environments were found to be more shielded than the signals associated with the monochalcogeno-, Ch_{mb}, and dichalcogeno-bridging, Ch_{db}, environments (Table 1) and contrast with the order observed for the $Sn_4Se_{10}^{4-}$ anion, i.e., $\delta(Se_t) > \delta(Se_{mb})$.[46] This difference can be rationalized using the rule of topological charge stabilization,[59] which predicts that the 4− charge of $Sn_4Se_{10}^{4-}$ is distributed over both the terminal and bridging atoms but is localized primarily on the terminal atoms in $Sn_2Ch_6^{4-}$ and $Sn_2Ch_7^{4-}$. For $Sn_2Se_7^{4-}$, the signal corresponding to Se_{mb} appeared at intermediate frequency, indicating a decrease in the shielding of the different selenium environments in the order $Se_t > Se_{mb} > Se_{db}$. The monoseleno- and diseleno-bridges each formally contribute a charge of 2− to the anions as "Se^{2-}" and "Se_2^{2-}", respectively. The selenium chemical shift of Se_2^{2-} is therefore expected to be less shielded than that of Se^{2-}. Accordingly, the chemical shift difference (Δ_1) between $\delta(Se_t)$ and $\delta(Se_{mb})$ (27.9 ppm) was found to be significantly smaller than the corresponding difference (Δ_2) between $\delta(Se_t)$ and $\delta(Se_{db})$ (174.9 ppm). For $Sn_2Te_7^{4-}$, however, Δ_1 (228.4 ppm) was found to be comparable in magnitude to Δ_2 (198.7 ppm). The differences between the relative ^{77}Se and ^{125}Te chemical shift ranges are qualitatively consistent with the larger dynamic range predicted for ^{125}Te by Ramsey's equation for nuclear shielding,[60] in which the paramagnetic term, σ^p, has a direct dependence on the radial term $\langle r^{-3}\rangle_{np}$ for the valence p-

(56) Huang, S.-P.; Dhingra, S.; Kanatzidis, M. G. *Polyhedron* **1990**, *9*, 1389.
(57) Dean, P. A. W.; Srivastava, R. S. *Inorg. Chim. Acta* **1985**, *105*, 1.
(58) Allen, L. C. *J. Am. Chem. Soc.* **1989**, *111*, 9003 and references therein.
(59) Gimarc, B. M.; Ott, J. S. *J. Am. Chem. Soc.* **1986**, *108*, 4298.
(60) Ramsey, N. F. *Phys. Rev.* **1950**, *78*, 699.

Table 2. Natural Abundance Isotopomers and Subspectra Used to Simulate the ^{119}Sn NMR Spectra of the $Sn_2Ch_6^{4-}$ (Ch = Se, Te) Anions

$^{119}Sn_x{}^{117}Sn_ySn_{2-x-y}$*$Ch_zCh_{6-z}^{4-}$ [a]			tot. intens, %[b]		multiplicity of subspectrum[c]
x	*y*	*z*	Se	Te	
1	0	0	8.962	8.800	S
1	0	1	1.470	1.501	S
1	0	1	1.470	1.501	d_t
1	0	1	1.470	1.501	d_{mb}
1	0	2	0.241	0.256	S
1	0	2	0.241	0.256	d_t
1	0	2	0.241	0.256	d_{mb}
1	0	2	0.060[d]	0.064[d]	d_t/d_{mb}[e]
1	1	0	0.814	0.799	D
1	1	1	0.134	0.136	D[f]
1	1	1	0.134	0.136	D/d_t[f]
1	1	1	0.134	0.136	D/d_{mb}[f]
2	0	0	0.917	0.901	S
2	0	1	0.301	0.307	d_t
2	0	1	0.150	0.154	d_{mb}

[a] *Ch denotes ^{77}Se or ^{125}Te. [b] Natural abundances of spin $^1/_2$ nuclides used to calculate isotopomer abundances were taken from ref 51: ^{77}Se, 7.58%; ^{117}Sn, 7.61%; ^{119}Sn, 8.58%; ^{125}Te, 6.99%. The natural abundances of ^{115}Sn (0.35%) and ^{123}Te (0.87%) are too low to contribute detectable isotopomer subspectra and are combined with the spinless tin and tellurium nuclides, respectively. [c] S denotes a singlet, D denotes a DOUBLET arising from $^2J(^{119}Sn-^{117}Sn)$, and d_t and d_{mb} denote doublets arising from $^1J(^{119}Sn-^{77}Se_t)$ and $^1J(^{119}Sn-^{77}Se_{mb})$, respectively. The symbols D/d_t and D/d_{mb} denote DOUBLET-of-doublets that result from a DOUBLET arising from $^2J(^{119}Sn-^{117}Sn)$ which, in turn, is split into a doublet by either $^1J(^{119}Sn-^{77}Se_t)$ or $^1J(^{119}Sn-^{77}Se_{mb})$, respectively. The doublet-of-doublets arising from $^1J(^{119}Sn-^{77}Se_t)$ and $^1J(^{119}Sn-^{77}Se_{mb})$ is denoted by d_t/d_{mb}. [d] Isotopomers having multiplet line intensities below this value are too weak to be observed and are not included in the summation of the simulated subspectra. [e] Not observed for $Sn_2Te_6^{4-}$. [f] Not observed.

Table 3. Natural Abundance Isotopomers and Subspectra Used to Simulate the ^{119}Sn NMR Spectra of the $Sn_2Ch_7^{4-}$ (Ch = Se, Te) Anions

$^{119}Sn_x{}^{117}Sn_ySn_{2-x-y}$*$Ch_zCh_{7-z}^{4-}$ [a]			tot. intens, %[b]		multiplicity of subspectrum[c]
x	*y*	*z*	Se	Te	
1	0	0	8.283	8.109	S
1	0	1	2.038	2.075	S
1	0	1	1.359	1.383	d_t
1	0	1	0.679	0.692	d_{mb}
1	0	1	0.679	0.692	d_{db}
1	0	2	0.206	0.219	S
1	0	2	0.413	0.437	d_t
1	0	2	0.206	0.219	d_{mb}
1	0	2	0.206	0.219	d_{db}
1	1	0	0.752	0.736	D[d]
1	1	1	0.216	0.251	D/d_t[e]
1	1	1	0.108	0.126	D/d_{mb}[e]
1	1	1	0.108	0.126	D/d_{db}[e]
2	0	0	0.848	0.830	S
2	0	1	0.278	0.283	d_t
2	0	1	0.070[f]	0.071[f]	d_{mb}
2	0	1	0.139	0.142	d_{db}

[a] *Ch denotes ^{77}Se or ^{125}Te. [b] Natural abundances of spin $^1/_2$ nuclides used to calculate isotopomer abundances were taken from ref 51: ^{77}Se, 7.58%; ^{117}Sn, 7.61%; ^{119}Sn, 8.58%; ^{125}Te, 6.99%. The natural abundances of ^{115}Sn (0.35%) and ^{123}Te (0.87%) are too low to contribute detectable isotopomer subspectra and are combined with the spinless tin and tellurium nuclides, respectively. [c] S denotes a singlet, D denotes a DOUBLET arising from $^2J(^{119}Sn-^{117}Sn)$, and d_t, d_{mb}, and d_{db} denote doublets arising from $^1J(^{119}Sn-^{77}Se_t)$, $^1J(^{119}Sn-^{77}Se_{mb})$, and $^1J(^{119}Sn-^{77}Se_{db})$, respectively. The symbols D/d_t, D/d_{mb}, and D/d_{db} denote DOUBLET-of-doublets that result from a DOUBLET arising from $^2J(^{119}Sn-^{117}Sn)$ which, in turn, is split into a doublet by either $^1J(^{119}Sn-^{77}Se_t)$, $^1J(^{119}Sn-^{77}Se_{mb})$, or $^1J(^{119}Sn-^{77}Se_{db})$, respectively. [d] Not observed for $Sn_2Te_7^{4-}$. [e] Not observed. [f] Isotopomers having multiplet line intensities below this value are too weak to be observed and are not included in the summation of the simulated subspectra.

electrons.[61,62] However, the shielding order for $Sn_2Te_7^{4-}$ was found to be $Te_t > Te_{db} > Te_{mb}$ and is reversed relative to that of the Se analogs. The apparently anomalous chemical shift ordering may be attributed to shielding anisotropy (SA)[63] and may also account for the shielding order observed for the $Sn_4Se_{10}^{4-}$ anion.[46] However, in the absence of a knowledge of the ^{77}Se and ^{125}Te shielding tensors, the apparent anomalies in the ^{77}Se and ^{125}Te shielding trends are presently not fully understood.

$SnCh_3^{2-}$ (Ch = Se, Te) Condensation Processes. Krebs and co-workers[14,31,64-67] observed a correlation between basicity and the extent of oligomerization of simple monomeric tin(IV) sulfide anions in aqueous solutions. For example, the monomeric SnS_4^{4-} anion was obtained from a strongly basic aqueous solution (pH = 11−12)[66] whereas the more condensed $Sn_2S_6^{4-}$ anion was obtained from a less basic solution (pH = 9−9.5).[65] The higher charge density of the smaller SnS_4^{4-} anion apparently renders it more basic and a better proton acceptor than $Sn_2S_6^{4-}$ and consequently requires a more basic medium for its stabilization. A similar correlation was also observed in the study of the GeS_4^{4-}, $Ge_2S_6^{4-}$, $Ge_2S_7^{4-}$, and $Ge_4S_{10}^{4-}$ anions in aqueous solutions.[14,68] In view of these results, we investigated the influence of ion-pair formation on the condensation of the $SnCh_3^{2-}$ (Ch = Se, Te) and $SnTe_4^{4-}$ anions in basic, nonaqueous solvents. This was accomplished by varying the relative amounts of unsequestered M^+ (M = Na, K) present in en or liquid NH_3 solutions of these anions.

Solutions obtained by extraction of the alloys $KSnCh_2$ (Ch = Se, Te) and NaSnTe in en in the presence of a stoichiometric excess of 2,2,2-crypt have been shown by multi-NMR spectroscopy to contain only the $SnCh_3^{2-}$ and $SnTe_4^{4-}$ anions, respectively.[28] Our study initially consisted of a systematic investigation by ^{119}Sn and ^{77}Se NMR spectroscopy of the extent of $SnSe_3^{2-}$ condensation in the presence of a nonstoichiometric amount of 2,2,2-crypt with respect to K^+. The en and liquid NH_3 extracts of the alloy $KSn_{0.67}Se_{1.93}$ containing a K^+:2,2,2-crypt stoichiometry of 1.00:0.42 were shown to contain the more condensed, less basic $Sn_2Se_6^{4-}$, $Sn_2Se_7^{4-}$, and $Sn_4Se_{10}^{4-}$ anions as major species along with a very small amount of the highly basic $SnSe_3^{2-}$ anion. This is consistent with the observation that the $Ge_2S_6^{4-}$ anion is always found in equilibrium with the $Ge_2S_7^{4-}$ and $Ge_4S_{10}^{4-}$ anions in strongly basic aqueous media.[68] The findings are supported by the X-ray crystal structure determinations of the $Sn_2Se_6^{4-}$ and $Sn_4Se_{10}^{4-}$ anions which were isolated from en extracts of the $KSn_{0.67}Se_{1.93}$ alloy (see **X-ray Crystal Structures** and ref 46). Nuclear magnetic resonance spectra of the liquid NH_3 extract of $KSn_{0.63}Te_{1.70}$ in the absence[47]

(61) Jameson, C. J.; Mason, J. In *Multinuclear NMR*; Mason, J., Ed.; Plenum Press: New York, 1987; Chapter 3, p 51.
(62) Webb, G. A. In *NMR and the Periodic Table*; Harris, R. K., Mann, B. E., Eds.; Academic Press: London, 1978; Chapter 3, p 49.
(63) Howarth, O. In *Multinuclear NMR*; Mason, J., Ed.; Plenum Press: New York, 1987; Chapter 5, p 149.
(64) Krebs, B.; Hürter, H.-U. *Z. Anorg. Allg. Chem.* **1980**, *462*, 143.
(65) Krebs, B.; Pohl, S.; Schiwy, W. *Z. Anorg. Allg. Chem.* **1972**, *393*, 241.
(66) Schiwy, W.; Pohl, S.; Krebs, B. *Z. Anorg. Allg. Chem.* **1973**, *402*, 77.
(67) Schiwy, W.; Blutau, C.; Gäthje, D.; Krebs, B. *Z. Anorg. Allg. Chem.* **1975**, *412*, 1.
(68) Pohl, S. Dissertation, Christian-Albrecht Universität, Kiel, Germany, 1974.

Table 4. Reduced Coupling Constants, K(Sn−Ch), and Relativistically Corrected Reduced Coupling Constants, $K(\mathrm{Sn-Ch})_{RC}$, for the $SnCh_4^{4-}$, $Sn_2Ch_6^{4-}$, $Sn_2Ch_7^{4-}$, and $SnCh_3^{2-}$ (Ch = Se, Te) Anions[a]

	K, $T^2\ J^{-1} \times 10^{20}$		K_{RC}, $T^2\ J^{-1} \times 10^{20}$	
anion	Sn−Ch	Sn−Sn	Sn−Ch	Sn−Sn
$SnTe_4^{4-}$	199.1[b]		97.1	
	206.5[c]		100.6	
$Sn_2Te_6^{4-}$ [d]	279.7 (t)		136.4 (t)	
	117.5 (mb)		57.3 (mb)	
$Sn_2Te_7^{4-}$ [d]	284.5 (t)		138.7 (t)	
	202.6 (mb)		98.8 (mb)	
	161.9 (db)		80.0 (db)	
$SnTe_3^{2-}$	316.6[b]		154.4	
	314.0[d]		153.1	
	305.8[c]		149.1	
$SnSe_4^{4-}$	169.8[b]		103.1	
$Sn_2Se_6^{4-}$	233.6 (t)[e]		141.9 (t)	
	101.2 (mb)[e]		61.5 (mb)	
	232.5 (t)[f]		141.3 (t)	
	103.0 (mb)[f]		62.6 (mb)	
$Sn_2Se_7^{4-}$	237.2 (t)[e]	16.60	144.1 (t)	8.2
	151.4 (mb)[e]		92.0 (mb)	
	131.0 (db)[e]		79.6 (db)	
	236.2 (t)[f]	18.70	143.5 (t)	9.2
	153.5 (mb)[f]		93.3 (mb)	
	131.5 (db)[f]		80.0 (db)	
$SnSe_3^{2-}$ [b]	237.8		144.5	

[a] The symbols t, mb, and db denote the terminal chalcogen and monochalcogeno- and dichalcogeno-bridging environments. [b] Recorded in en solvent (24 °C) containing a stoichiometric excess of 2,2,2-crypt with respect to K^+.[28] [c,d] In NH_3 solvent (−70 °C) containing unsequestered Na^+ [K^+]. [e,f] Recorded in en [NH_3] solvent (0 [−50] °C containing a stoichiometric excess[28] [absence] of 2,2,2-crypt with respect to K^+.

of 2,2,2-crypt established the presence of the $Sn_2Te_6^{4-}$ and $Sn_2Te_7^{4-}$ anions in solution along with comparable amounts of $SnTe_3^{2-}$. No conclusive evidence was found for the $Sn_4Te_{10}^{4-}$ anion. The liquid NH_3 extract of $NaSn_{0.43}Te$ in the absence of 2,2,2-crypt was shown to contain primarily the $SnTe_4^{4-}$ anion along with a small amount of $SnTe_3^{2-}$.

Condensation of the monomeric $SnCh_3^{2-}$ anions can be viewed as the nucleophilic attack of a Ch atom of one monomer on the Sn center of another and is sterically favored by the trigonal-planar (D_{3h}) geometry of the anions. The lack of condensation of the $SnTe_4^{4-}$ anion may be a consequence of the more sterically crowded tetrahedral environment as well as the higher anion charge. This process can also be rationalized in terms of ion-pairing and charge stabilization in the monomeric and oligomeric anions. Condensation according to eq 4 results

$$n\mathrm{SnCh_3}^{2-}\ (+\ \mathrm{M}^+) \rightleftharpoons \mathrm{SnCh_3}^{2-} + \mathrm{Sn_2Ch_6}^{4-} + \mathrm{Sn_2Ch_7}^{4-} + \mathrm{Sn_4Ch_{10}}^{4-}\ (+\ \mathrm{M}^+) \quad (4)$$

in the localization of the 4− charge at the Ch_t positions of the more condensed anions. Formally, the charge per Ch_t atom is 1− in the oligomeric anions and $^2/_3$− in $SnCh_3^{2-}$. The free M^+ cations strongly ion-pair in solution with (a) the Ch atoms of $SnCh_3^{2-}$, reducing anionic−anionic repulsions and allowing the monomeric species to condense, and (b) the Ch_t atoms of the more condensed species, stabilizing the higher formal charges on these atoms. In essence, the M^+ cation plays the role of a proton in the condensation of the $SnCh_3^{2-}$ anions (cf. the condensation of SnS_4^{4-} and GeS_4^{4-} as a function of pH in aqueous solutions; see refs 14, 31, and 64−67 and above). The larger oligomeric:monomeric anion ratio observed in the Sn/Se system when compared to that of the Sn/Te system can be explained in terms of the electronegativity difference between Se and Te.[58] The higher electronegativity of Se when compared to that of Te renders the Sn−Se bond more ionic and enhances the formation of oligomers by means of nucleophilic attack, and may account for the formation of the $Sn_4Ch_{10}^{4-}$ tetramer in the Sn/Se system but not in the Sn/Te system.

The differences between the present and previously reported[28] $\delta(^{119}\mathrm{Sn})$, $\delta(^{125}\mathrm{Te})$, and $^1J(^{119}\mathrm{Sn}-^{125}\mathrm{Te})$ values for the $SnTe_3^{2-}$ anion (Table 1) can be attributed to strong ion-pairing between M^+ and $SnTe_3^{2-}$. Ion-pairing leads to deshielding of the Sn center and shielding of the Te nucleus as well as to a decrease in $^1J(^{119}\mathrm{Sn}-^{125}\mathrm{Te})$, indicating removal of s-electron density from the Sn−Te bonds. Moreover, $^1J(^{119}\mathrm{Sn}-^{125}\mathrm{Te})$ was noted to be a function of ion-pairing and decreased according to the polarizing ability of M^+, i.e., $^1J(^{119}\mathrm{Sn}-^{125}\mathrm{Te})$ decreased in the order 2,2,2-crypt-$K^+\cdots[SnTe_3^{2-}]$ (negligible ion-pairing) > $K^+\cdots[SnTe_3^{2-}]$ > $Na^+\cdots[SnTe_3^{2-}]$. A similar trend in $\delta(^{119}\mathrm{Sn})$ and $^1J(^{119}\mathrm{Sn}-^{117}\mathrm{Sn})$ was noted for the series of cluster anions $Sn_{9-n}Pb_n^{4-}$ and $Sn_{9-n}Ge_n^{4-}$ (n = 0−8) in en solutions containing unsequestered alkali-metal cations.[69]

The ^{119}Sn and ^{125}Te NMR spectra (−70 °C) of the $SnTe_3^{2-}$ anion in liquid NH_3 extracts of M/Sn/Ch (M = Na, K) alloys containing no 2,2,2-crypt were recorded at 11.744 and 7.0463 T and gave rise to significantly larger line widths ($\nu_{1/2}$) at the higher external field strength (B_o), i.e., 75.5 (^{119}Sn) and 62.5 (^{125}Te) Hz at 11.744 T compared with 55.5 (^{119}Sn) and 32.8 (^{125}Te) Hz at 7.0463 T. This indicates that relaxation by means of the shielding anisotropy (SA) mechanism,[63] which varies with B_o^2 [(11.744 T)^2/(7.0463 T)^2 = 2.78], makes an important contribution to the spin−lattice relaxation of ^{119}Sn [(75.5 Hz)/(55.5 Hz) = 1.36] and ^{125}Te [(62.5 Hz)/(32.8 Hz) = 1.91] in $SnTe_3^{2-}$. The influence of ion-pairing on line broadening is also known[70] and may also contribute to the broadening of the ^{119}Sn and ^{125}Te signals of the $SnTe_3^{2-}$ anion by means of chemical exchange, the SA effect, and other relaxation mechanisms.

(II) X-ray Crystal Structures of $K^+(N(CH_3)_4^+)_3Sn_2Se_6^{4-}$ (1), $(enH^+)_2$(2,2,2-crypt-$K^+)_2Sn_2Se_6^{4-}$ (2), $(K^+)_2$(2,2,2-crypt-$K^+)_2Sn_2Te_6^{4-}$ (3), K^+(2,2,2-crypt-$K^+)_2HOSnTe_3^{3-}$ (4), and K^+(2,2,2-crypt-$K^+)_2HOSnTe_3^{3-}$·en (5). Details of the data collection parameters and other crystallographic information are given in Table 5. The final atomic coordinates and equivalent isotropic thermal parameters for the non-hydrogen atoms are summarized in Table 6. The most significant bond distances and angles in the $Sn_2Ch_6^{4-}$ (Ch = Se, Te) anions, the long contact distances in the $K^+\cdots Sn_2Ch_6^{4-}$ units, and significant bond distances and angles in the $HOSnTe_3^{3-}$ anion are listed in Table 7.

In the five compounds, the structures of the $N(CH_3)_4^+$ and 2,2,2-crypt-K^+ cations are similar to those determined previously for symmetry-unconstrained units in $N(CH_3)_4^+Bi(OTeF_5)_6^-$,[71] K^+(2,2,2-crypt-$K^+)_3Pb_9^{4-}$,[72] and (2,2,2-crypt-$K^+)_2Sn_2Se_3^{2-}$ [55] with average N−C bond lengths of 1.48(6) Å for **1** and average K···O, K···N distances of 2.82(1), 3.00(1) Å for **2**, and 2.81(2) [2.81(3)], 2.96(1) [2.96(2)] Å for **4** [**5**] (also see **Experimental Section, Solution and Refinement of the Structures** for **3**). A complete list of bond distances and angles in the $N(CH_3)_4^+$

(69) Wilson, W. L.; Rudolph, R. W.; Lohr, L. L.; Taylor, R. C.; Pyykkö, P. *Inorg. Chem.* **1986**, *25*, 1535.
(70) Björgvinsson, M.; Schrobilgen, G. J. *Inorg. Chem.* **1991**, *30*, 2540.
(71) Mercier, H. P. A.; Sanders, J. C. P.; Schrobilgen, G. J. *J. Am. Chem. Soc.* **1994**, *116*, 2921.
(72) Campbell, J.; Dixon, D. A.; Mercier, H. P. A.; Schrobilgen, G. J. *Inorg. Chem.* **1995**, *34*, 5798.

Table 5. Summary of Crystal Data and Refinement Results for $K^+(N(CH_3)_4^+)_3Sn_2Se_6^{4-}$ (**1**), $(enH^+)_2(2,2,2\text{-crypt-}K^+)_2Sn_2Se_6^{4-}$ (**2**), $(K^+)_2(2,2,2\text{-crypt-}K^+)_2Sn_2Te_6^{4-}$ (**3**), $K^+(2,2,2\text{-crypt-}K^+)_2HOSnTe_3^{3-}$ (**4**), and $K^+(2,2,2\text{-crypt-}K^+)_2HOSnTe_3^{3-}\cdot$en (**5**)

	1	**2**	**3**	**4**	**5**
space group (No.)	$P\bar{1}$ (2)	$P2_1/n$ (14)	$P\bar{1}$ (2)	$P\bar{1}$ (2)	$P\bar{1}$ (2)
a Å	9.587(3)	8.442(2)	11.025(5)	11.670(2)	14.774(6)
b, Å	10.005(2)	25.877(5)	11.118(7)	12.977(4)	15.161(5)
c, Å	15.996(5)	14.821(3)	17.137(9)	18.628(5)	16.744(5)
α, deg	95.15(2)	90.00	95.09(5)	94.14(2)	71.25(3)
β, deg	92.81(2)	104.19(3)	107.22(4)	106.21(2)	68.41(3)
γ, deg	106.96(2)	90.00	109.49(4)	100.49(2)	62.41(3)
V, Å^3	1457.1(7)	3138.9(12)	1850(2)	2641(1)	3038(2)
molecules/unit cell	2	2	1	2	2
mol wt	972.68	1664.54	1912.36	1388.87	1448.88
calcd density, g cm^{-3}	2.217	1.761	1.717	1.746	1.584
T, °C	24	−100	24	−105	24
color	yellow	yellow	deep red	orange	deep red
μ, cm^{-1}	49.49	23.64	17.2	12.7	11.1
λ, Å	0.560 86	0.560 86	0.560 86	0.560 86	0.560 86
R_1[a] (wR_2[b])	0.0494 (0.1223)	0.0396 (0.0918)	0.1172 (0.2961)	0.0554 (0.0762)	0.0553 (0.1621)

[a] $R_1 = \sum||F_o| - |F_c||/\sum|F_o|$. [b] $wR_2 = [\sum[w(F_o^2 - F_c^2)^2]/\sum w(F_o^2)^2]^{1/2}$.

and 2,2,2-crypt-K^+ cations is given in the Supporting Information, Table S2.

$Sn_2Ch_6^{4-}$ (Ch = Se, Te) in 1−3. The crystal structure of **1** consists of well-separated $N(CH_3)_4^+$ cations and infinite chains of $-K-(Sn_2Se_6)-K-(Sn_2Se_6)-K-$ in which the anions are bridged by K^+ cations running parallel to the diagonal of the cell. Each $Sn_2Se_6^{4-}$ anion is bridged *cis* or *trans* to the plane passing through the Sn and bridging Se atoms (Figure 5). Accordingly, each K^+ cation bridges four terminal Se atoms (two *cis* and two *trans*) of two anions, completing a distorted tetrahedral environment about the K^+ cation. The K^+ cation is in the same plane as the Sn atoms at a distance of 4.039(4) Å when bridging *cis* and 3.971(5) Å when bridging *trans*. The K···Se distances [3.326(3)−3.369(3) Å] are at the limit of the sum of the K^+ ionic (1.33 Å)[73] and the Se van der Waals radii (2.0 Å)[73] of 3.33 Å and are comparable to those observed in $K_4Sn_2Se_6$ [3.301−3.531 Å].[32] The $N(CH_3)_4^+\cdots Se_b$ [5.055(5)−5.366(5) Å] and $N(CH_3)_4^+\cdots Se_t$ [4.307(5)−4.349(5) Å] distances are shorter than the sum of the $N(CH_3)_4^+$ (3.48−3.50 Å)[71] and Se van der Waals radii (2.0 Å) of 5.48−5.50 Å.

The crystal structure of **2** consists of well-separated 2,2,2-crypt-K^+ cations and protonated en solvent molecules, $H_2N(CH_2)_2NH_3^+$. Two protonated en solvent molecules are hydrogen-bonded to the Se_b and Se_t atoms of the $Sn_2Se_6^{4-}$ anions (Figure 5). The N−H···Se distances [3.374(5) and 3.570(4) Å for N−H···Se_t and 3.735(5) Å for N−H···Se_b] are comparable to those observed in $(enH_2)_2Sn_2Se_6\cdot$en [3.426−3.799 Å].[35]

The crystal structure of **3** consists of two 2,2,2-crypt-K^+ cations and one $Sn_2Te_6^{4-}$ anion bridging two symmetry-related K^+ cations, forming layers of $K-(Sn_2Te_6)-K$ (Figure 5). Alternatively, each K^+ cation is in contact with the Te_t and the Te_{mb} atoms of one anion and is in the same plane as the two Sn atoms at an average distance of 4.21(1) Å. The K···Te distances are in the range 3.580(11)−3.778(11) Å and are slightly longer than the sum of the K^+ ionic radius (1.33 Å)[73] and the Te van der Waals radius (2.2 Å)[73] of 3.53 Å. The K···K distances between $K-(Sn_2Te_6)-K$ units is 3.79(1) Å, and the distance within a unit is 7.48(1) Å.

The structures of the $Sn_2Ch_6^{4-}$ anions (Ch = Se, Te) are based on two edge-sharing distorted $SnCh_4$ tetrahedra and are therefore isostructural with B_2H_6,[74] $W_2Se_6^{2-}$,[75] and $Ge_2Ch_6^{4-}$ (Ch = S,[68] Se,[76]). The two distinct Sn−Ch bond distances, i.e., $Sn-Ch_t$ and $Sn-Ch_{mb}$, are slightly shorter and longer, respectively, than those found in the crystal structures of $SnCh_4^{4-}$ [Se, 2.494(1)−2.536(1) Å;[29] Te, 2.710(3)−2.819(2) Å[30]]. The average $Sn-Ch_t$ distances [Se, 2.460(4) Å in **1** and 2.460(1) Å in **2**; Te, 2.669(4) Å] are significantly shorter than the average $Sn-Ch_{mb}$ distances [Se, 2.598(4) Å in **1** and 2.582(1) Å in **2**; Te, 2.817(3) Å] and are consistent with the expected higher relative bond order of the $Sn-Ch_t$ bonds. Similar average $Sn-Ch_t$ and $Sn-Ch_{mb}$ bond distances were also observed in the previously reported $Sn_2Ch_6^{4-}$ structures.[77] These distances correlate well with the larger $^1K(Sn-Ch_t)_{RC}$ and smaller $^1K(Sn-Ch_{mb})_{RC}$ couplings determined for the $Sn_2Ch_6^{4-}$ anions (see **Coupling Constants**). In the present $Sn_2Se_6^{4-}$ anion structures, the Sn···Sn distances [3.602(3) Å in **1** and 3.557(1) Å in **2**] are most similar to the Sn···Sn distances reported for $Na_4Sn_2Se_6\cdot 13H_2O$ [3.529(1) Å][31] but are longer than those observed in $K_4Sn_2Se_6$ [3.514 Å],[32] $Cs_4Sn_2Se_6$ [3.504(1) Å],[34] $Rb_4Sn_2Se_6$ [3.518 Å],[33] and $(enH_2)_2Sn_2Se_6\cdot$en [3.480(1) Å].[35] The Sn···Sn distance in the present $Sn_2Te_6^{4-}$ anion [3.865(3) Å] is longer than those reported for the $N(CH_3)_4^+$ [3.782(2) Å][27] and $N(C_2H_5)_4^+$ [3.781(2) Å][36] salts. The average $Se_b-Sn-Se_b$, $Sn-Se_b-Sn$ bond angles in the present $Sn_2Se_6^{4-}$ structures [92.47(7), 86.06(7)°] are most similar to those observed in $Na_4Sn_2Se_6\cdot 13H_2O$ [93.9(1), 86.1(1)°] but differ from those in $K_4Sn_2Se_6$ [94.5, 85.5°], $Cs_4Sn_2Se_6$ [94.74(5), 85.26(5)°], $Rb_4Sn_2Se_6$ [94.6(1), 85.4°], and $(enH_2)_2Sn_2Se_6\cdot$en [95.1(1), 84.9(1)°]. The present $Te_b-Sn-Te_b$ [93.41(9)°] and $Sn-Te_b-Sn$ [86.59(9)°] bond angles are smaller and larger, respectively, than those observed in the $N(CH_3)_4^+$ [95.0(9), 85.0(1)°] and $N(C_2H_5)_4^+$ [95.4(1), 84.8(1)°] salts.

$HOSnTe_3^{3-}$ in 4 and 5. The $HOSnTe_3^{3-}$ anion was obtained during an attempt to obtain crystals of the trigonal-bipyramidal cage anion $TlSnTe_3^{3-}$ from an en solution prepared by reacting the alloys $Tl_2Sn_2Te_3$ and K_2Te in the presence of a stoichiometric excess of 2,2,2-crypt.[78] The en solution was shown by ^{119}Sn and ^{125}Te NMR spectroscopy to contain small amounts of the $Tl_2Te_2^{2-}$, $SnTe_3^{2-}$, and HTe^- anions as well as larger

(73) Pauling, L. *The Nature of the Chemical Bond*, 3rd ed.; Cornell University Press: Ithaca, NY, 1960; pp 224, 257, 260, 514.
(74) Greenwood, N. N.; Earnshaw, A. *Chemistry of the Elements*; Pergamon Press: Oxford, U.K., 1984; Chapter 6, pp 174, 181.
(75) Lu, Y.-J.; Ansari, M. A.; Ibers, J. A. *Inorg. Chem.* **1989**, *28*, 4049.
(76) Krebs, B.; Müller, H. *Z. Anorg. Allg. Chem.* **1983**, *496*, 47.
(77) $Na_4Sn_2Se_6\cdot 13H_2O$ [t, 2.470(1) Å; mb, 2.586(1) Å],[31] $K_4Sn_2Se_6$ [t, 2.461 Å; mb, 2.588 Å],[32] $Rb_4Sn_2Se_6$ [t, 2.462(4) Å; mb, 2.594(5) Å],[33] $Cs_4Sn_2Se_6$ [t, 2.450(2) Å; mb, 2.587(1) Å],[34] $(enH_2)_2Sn_2Se_6\cdot$en [t, 2.460(1) Å; mb, 2.579(1) Å],[35] $(N(CH_3)_4)_4Sn_2Te_6$ [t, 2.694(2) Å; mb, 2.799(1) Å],[27] $(N(C_2H_5)_4)_4Sn_2Te_6$ [t, 2.685(1) Å; mb, 2.809(4) Å],[36] and $Cs_4Sn_2Te_7$ [t, 2.683(3) Å; mb, 2.808(2) Å].[50]
(78) Campbell, J.; Czyborra, R.; Mercier, H. P. A.; Pirani, A. M.; Schrobilgen, G. J. *Inorg. Chem.*, to be submitted.

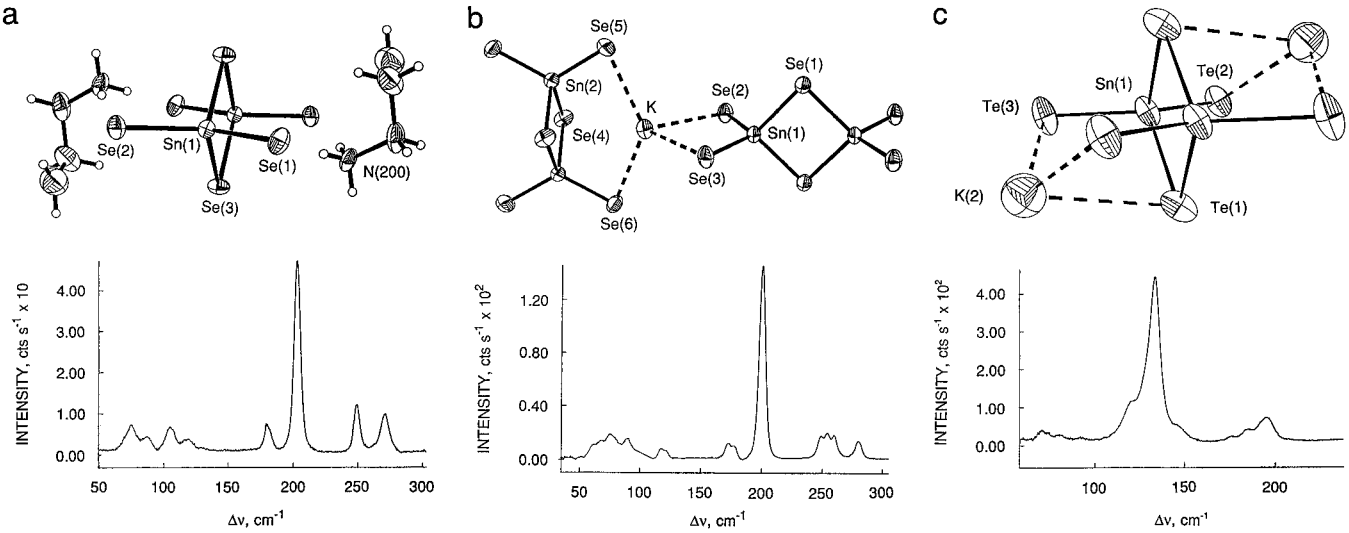

Figure 5. ORTEP views and Raman spectra of (a) $Sn_2Se_6^{4-}$ in $(enH^+)_2$(2,2,2-crypt-$K^+)_2Sn_2Se_6^{4-}$, (b) $Sn_2Se_6^{4-}$ in $K^+(N(CH_3)_4^+)_3Sn_2Se_6^{4-}$, and (c) $Sn_2Te_6^{4-}$ in $(K^+)_2$(2,2,2-crypt-$K^+)_2Sn_2Te_6^{4-}$. Thermal ellipsoids are shown at the 50% ($Sn_2Se_6^{4-}$) and at the 30% ($Sn_2Te_6^{4-}$) probability levels.

amounts of $TlSnTe_3^{3-}$ and a new Sn(IV)/Te anion. The structure of the new Sn(IV)/Te anion could not be determined, but the observed I_S/I_C intensity ratio and the magnitude of $^1K(Sn-Te)_{RC}$, 146.6 $T^2\ J^{-1} \times 10^{20}$, which is comparable to the $^1K(Sn-Te)_{RC}$ value determined for $SnTe_3^{2-}$ (154.4 $T^2\ J^{-1} \times 10^{20}$), suggested that the anion contains $SnTe_3$ units. Only the $HOSnTe_3^{3-}$ anion was characterized by X-ray crystallography in the crystalline material obtained from the en solution. It is therefore reasonable to speculate that the solution species is $HOSnTe_3^{3-}$.

Although the synthesis of the $HOSnTe_3^{3-}$ anion appears to be adventitious, reduction of 2,2,2-crypt by the strong reducing agent K_2Te has been noted before[70] and likely serves as a hydroxide ion source leading to the formation of compounds **4** and **5**. Compounds **4** and **5** were obtained from a solution prepared by using a slight excess of 2,2,2-crypt with respect to K^+, yet both structures contain unsequestered K^+, which is consistent with attack on the cryptand.

The Sn−Te distances in the $HOSnTe_3^{3-}$ anion (Figure 6) range from 2.674(1) to 2.710(1) [average 2.696(2)] Å in **4** and from 2.683(2) to 2.707(2) [average 2.696(3)] Å in **5**. The average Sn−Te bond distance is shorter than the average Sn−Te_t distance in $Sn_2Te_6^{6-}$ [2.727(2) Å][43] and those in $SnTe_4^{4-}$ [2.710(3)−2.819(2) Å][30] and is comparable to the average Sn−Te_t distances in $Sn_2Te_6^{4-}$ [2.669(4) Å] and $Sn_2Te_7^{4-}$ [2.683(3) Å]. In addition, the present Sn−Te distances are shorter than the sum of the Te covalent radius (1.37 Å)[73] and the Sn(IV) metallic radius (1.399 Å)[73] of 2.77 Å. The Sn−O distances [2.081(5) Å in **4** and 2.027(8) Å in **5**] are longer than the average Sn−O bond distance [1.948(3) Å] observed in the crystal structure of Sn(O-*t*-Bu)$_4$,[79] but are comparable to the sum of the O single-bond covalent radius (0.66 Å)[73] and the Sn(IV) metallic radius (1.399 Å) of 2.06 Å. The Te−Sn−Te bond angles range from 116.25(3) to 118.21(3)° in **4** and from 114.54(5) to 119.82(5)° in **5**, and the Te−Sn−O bond angles are in the ranges 96.1(2)−107.6(2)° in **4** and 96.2(2)−105.5(2)° in **5**.

The $HOSnTe_3^{3-}$ anion is the first example of a simple mixed hydroxytellurate anion of tin and is structurally related to $OWTe_3^{2-}$ [80] and isostructural with $HOGeS_3^{3-}$.[81] The $HOSnTe_3^{3-}$ anion can be formally viewed as being obtained by the nucleophilic attack of OH^- on the Sn atom of the trigonal-planar $SnTe_3^{2-}$ anion. The nucleophilic attack induces a change in the hybridization of the Sn atom from pure sp^2 in the $SnTe_3^{2-}$ anion to ca. sp^3 in $HOSnTe_3^{3-}$ and is accompanied by a slight distortion of the D_{3h} geometry of $SnTe_3^{2-}$ to C_{3v} point symmetry (the tin atoms are 0.468 (**4**) and 0.454 Å (**5**) above the center of the plane containing the three Te atoms). This distortion is reflected in the magnitudes of the average Te−Sn−Te bond angles [117.06(5)° in **4** and 117.25(9)° in **5**], which are smaller than the ideal D_{3h} angles of 120°. By analogy with the $Sn_2Ch_6^{4-}$ and $Sn_2Ch_7^{4-}$ (Ch = Se, Te) anions, the 3− charge on the $HOSnTe_3^{3-}$ anion is expected to be localized on the Te atoms.

(III) Structural Characterization of the $Sn_2Ch_6^{4-}$ (Ch = Se, Te) Anions by Raman Spectroscopy. The solid-state Raman spectra of $(enH^+)_2$(2,2,2-crypt-$K^+)_2Sn_2Se_6^{4-}$, $K^+(N(CH_3)_4^+)_3Sn_2Se_6^{4-}$, and $(K^+)_2$(2,2,2-crypt-$K^+)_2Sn_2Te_6^{4-}$ are shown in Figure 5. The observed frequencies and their assignments are summarized in Tables 8 and 9. Assignments for the en solvent molecule and for the 2,2,2-crypt-K^+ and $N(CH_3)_4^+$ cations were made by comparison with values reported for the solid state Raman spectra of en,[85] (2,2,2-crypt-K^+)I^-,[86] and $N(CH_3)_4^+$ [71] and are not given in Tables 8 and 9. The vibrational modes of the $Sn_2Se_6^{4-}$ and $Sn_2Te_6^{4-}$ anions were assigned under D_{2h} point symmetry and belong to the irreducible representations $\Gamma_{vib} = 4A_g + 2B_{1g} + 2B_{2g} + B_{3g} + A_u + 3B_{1u} + 2B_{2u} + 3B_{3u}$. A total of 18 vibrational bands are expected, of which nine modes (A_g, B_{1g}, B_{2g}, and B_{3g}) are Raman active,

(79) Hampden-Smith, M. J.; Wark, T. A.; Rheingold, A.; Huffman, J. C. *Can. J. Chem.* **1991**, *69*, 121.
(80) Gardner, D. R.; Fettinger, J. C.; Eichhorn, B. W. *Angew. Chem., Int. Ed. Engl.* **1994**, *33*, 1859.
(81) Krebs, B.; Wallstab, H.-J. *Inorg. Chim. Acta* **1981**, *54*, L123.
(82) Beattie, I. R.; Gilson, T.; Cocking, P. *J. Chem. Soc. A* **1967**, 702.
(83) Balls, A.; Downs, A. J.; Greenwood, N. N.; Straughan, B. P. *Trans. Faraday Soc.* **1966**, *62*, 521.
(84) Beattie, I. R.; Gilson, T.; Ozin, G. A. *J. Chem. Soc. A* **1968**, 814.
(85) Giorgini, M. G.; Pelletti, M. R.; Paliani, G.; Cataliotti, R. S. *J. Raman Spectrosc.* **1983**, *14*, 16. No en bands are found within the frequency window containing the $Sn_2Se_6^{4-}$ bands.
(86) The solid state Raman spectrum of microcrystalline (2,2,2-crypt-K^+)-I^- was recorded at room temperature under the same conditions used to record the spectra of the $Sn_2Ch_6^{4-}$ (Ch = Se, Te) salts. The Raman spectrum of (2,2,2-crypt-K^+)I^- displayed four weak, broad bands in the 50−300 cm^{-1} region, i.e., 94 (33), 135 (100), 175 (42), 216 (17) cm^{-1}. The most intense 2,2,2-crypt-K^+ band at 135 cm^{-1}, which does not overlap with any $Sn_2Se_6^{4-}$ anion bands, was too weak to be observed in the Raman spectrum of $(enH^+)_2$(2,2,2-crypt-$K^+)_2Sn_2Se_6^{4-}$.
(87) See ref 31. Six bands were reported for the Raman spectrum of $Na_4Sn_2Se_6 \cdot 13H_2O$: 260, 202, 188, 116, 93, 78 cm^{-1} (relative intensities not given).

Table 6. Atomic Coordinates ($\times 10^4$) and Equivalent Isotropic Displacement Parameters (Å^2 $\times$ 10^3) for $K^+(N(CH_3)_4^+)_3Sn_2Se_6^{4-}$, $(enH^+)_2(2,2,2\text{-crypt-}K^+)_2Sn_2Se_6^{4-}$, $(K^+)_2(2,2,2\text{-crypt-}K^+)_2Sn_2Te_6^{4-}$, $K^+(2,2,2\text{-crypt-}K^+)_2HOSnTe_3^{3-}$, and $K^+(2,2,2\text{-crypt-}K^+)_2HOSnTe_3^{3-}\cdot en$[a]

	x	y	z	U_{eq}		x	y	z	U_{eq}
				$K^+(N(CH_3)_4^+)_3Sn_2Se_6^{4-}$					
Sn(1)	966(1)	597(1)	943(1)	32(1)	C(103)	4310(21)	1961(27)	684(14)	131(9)
Se(1)	−1341(1)	3799(1)	631(1)	42(1)	C(104)	3149(26)	715(21)	−661(13)	123(8)
Se(2)	2988(1)	5406(1)	1698(1)	43(1)	N(200)	3022(12)	3932(11)	6792(7)	47(3)
Se(3)	451(2)	8059(1)	1654(1)	45(1)	C(201)	3182(15)	2667(13)	7176(9)	49(3)
Sn(2)	3963(1)	8689(1)	5615(1)	37(1)	C(202)	4292(15)	4475(16)	6274(10)	64(4)
Se(4)	6556(2)	9214(1)	5056(1)	47(1)	C(203)	2978(20)	5017(15)	7454(12)	81(6)
Se(5)	2241(2)	6553(2)	4880(1)	66(1)	C(204)	1585(16)	3461(17)	6231(10)	68(5)
Se(6)	4226(2)	9087(2)	7159(1)	48(1)	N(300)	727(12)	2039(12)	3131(7)	50(3)
K	6961(3)	1898(3)	6866(2)	51(1)	C(301)	−119(19)	2035(23)	2353(13)	114(8)
N(100)	3191(14)	1837(13)	0(8)	62(3)	C(302)	944(34)	3340(17)	3664(14)	188(17)
C(101)	1779(16)	1615(17)	377(10)	66(4)	C(303)	2157(16)	1909(18)	2847(11)	79(5)
C(102)	3483(19)	3222(16)	−352(10)	79(6)	C(304)	−8(16)	817(16)	3577(10)	68(5)
				$(enH^+)_2(2,2,2\text{-crypt-}K^+)_2Sn_2Se_6^{4-}$					
Sn(1)	−356(1)	−386(1)	923(1)	22(1)	C(113)	883(11)	2658(3)	6164(6)	61(2)
Se(1)	−2997(1)	−835(1)	721(1)	35(1)	C(114)	1508(12)	2198(4)	6732(5)	68(3)
Se(2)	1741(1)	−499(1)	2381(1)	32(1)	O(115)	1253(7)	1750(2)	6156(3)	48(1)
Se(3)	−864(1)	572(1)	489(1)	29(1)	C(116)	1724(11)	1295(3)	6706(5)	52(2)
K(1)	2501(2)	1865(1)	4574(1)	30(1)	C(117)	1444(11)	828(3)	6094(5)	52(2)
N(100)	2484(7)	815(2)	5433(4)	41(1)	C(118)	4161(10)	671(3)	5905(5)	60(2)
C(101)	1844(10)	448(3)	4690(5)	46(2)	C(119)	5406(10)	792(4)	5374(6)	61(2)
C(102)	350(9)	617(3)	3984(5)	44(2)	O(120)	5462(6)	1336(2)	5248(4)	57(1)
O(103)	686(5)	1079(2)	3541(3)	33(1)	C(121)	6749(11)	1476(4)	4834(6)	71(3)
C(104)	−616(9)	1227(3)	2779(4)	40(2)	C(122)	6885(11)	2036(5)	4810(7)	84(3)
C(105)	−24(9)	1627(3)	2224(4)	40(2)	O(123)	5472(7)	2239(3)	4241(4)	69(2)
O(106)	386(6)	2078(2)	2778(3)	40(1)	C(124)	5544(12)	2789(4)	4198(6)	72(3)
C(107)	1004(12)	2472(3)	2280(4)	56(2)	C(125)	4140(11)	2981(4)	3471(5)	64(3)
C(108)	1242(12)	2957(3)	2849(5)	64(3)	N(200)	−5630(6)	40(2)	1210(3)	33(1)
N(109)	2555(8)	2912(2)	3713(4)	47(2)	C(201)	−4518(8)	432(3)	1765(4)	47(2)
C(110)	2340(12)	3317(3)	4368(5)	57(2)	C(202)	−5504(10)	867(4)	2088(5)	59(2)
C(111)	1170(10)	3183(3)	4921(5)	54(2)	N(203)	−6126(9)	700(3)	2852(4)	68(2)
O(112)	1744(6)	2740(2)	5492(3)	41(1)					
				$(K^+)_2(2,2,2\text{-crypt-}K^+)_2Sn_2Te_6^{4-}$					
Sn(1)	4260(2)	4322(2)	8809(1)	66(1)	C(10)	−1875(21)	1046(14)	7862(9)	250(8)
Te(1)	3619(2)	3365(2)	10166(1)	86(1)	C(11)	−443(19)	1434(10)	7901(9)	250(8)
Te(2)	5261(2)	2805(2)	8112(1)	82(1)	O(12)	−114(13)	297(11)	7797(6)	202(6)
Te(3)	2250(2)	4925(3)	7848(1)	99(1)	C(13)	1281(12)	600(14)	7996(8)	250(8)
K(2)	1770(11)	5493(14)	9924(6)	165(4)	C(14)	1572(9)	−595(17)	7877(9)	250(8)
K(1)	−1850(6)	−1651(6)	6377(3)	82(2)	O(16)	952(6)	−1230(14)	7019(9)	202(6)
N(1)	−838(15)	−3557(12)	5696(9)	206(13)	C(16)	1318(11)	−2330(18)	6878(12)	250(8)
C(1)	−1422(19)	−3825(15)	4790(9)	250(8)	C(17)	665(15)	−2984(17)	5974(12)	250(8)
C(2)	−1370(20)	−2661(17)	4408(7)	250(8)	C(18)	−1303(19)	−4769(11)	5992(11)	250(8)
O(3)	−2106(15)	−2002(14)	4707(4)	202(6)	C(19)	−2756(18)	−5223(6)	5959(11)	250(8)
C(4)	−2249(19)	−980(17)	4291(5)	250(8)	O(20)	−2900(13)	−4275(7)	6501(9)	202(6)
C(5)	−3295(17)	−568(17)	4486(7)	250(8)	C(21)	−4228(14)	−4273(11)	6562(11)	250(8)
O(6)	−2801(14)	−15(12)	5351(8)	202(6)	C(22)	−4291(14)	−3795(15)	7188(11)	250(8)
C(7)	−3791(17)	368(15)	5574(11)	250(8)	O(23)	−4112(11)	−2619(14)	6933(9)	202(6)
C(8)	−3165(19)	1079(13)	6468(12)	250(8)	C(24)	−4160(16)	−1674(18)	7530(10)	250(8)
N(9)	−2889(16)	231(13)	7059(9)	206(13)	C(25)	−4190(17)	−517(18)	7173(11)	250(8)
				$K^+(2,2,2\text{-crypt-}K^+)_2HOSnTe_3^{3-}$					
Sn(1)	−1461(1)	−5912(1)	8170(1)	22(1)	O(123)	−118(5)	−2874(4)	4297(3)	28(1)
Te(1)	788(1)	−4653(1)	8482(1)	32(1)	C(124)	956(7)	−3204(7)	4690(5)	35(2)
Te(2)	−3329(1)	−4936(1)	8144(1)	30(1)	C(125)	1566(8)	−2488(7)	5427(6)	44(3)
Te(3)	−1904(1)	−7683(1)	7220(1)	29(1)	K(2)	−3150(2)	−1395(2)	9348(1)	26(1)
O(1)	−1239(5)	−6338(4)	9249(3)	30(2)	N(200)	−4044(6)	−1325(6)	7724(4)	30(2)
K(3)	−1046(2)	−4164(2)	9860(1)	33(1)	C(201)	−4872(9)	−573(7)	7564(5)	40(3)
K(1)	−1658(2)	−2334(1)	5094(1)	25(1)	C(202)	−4359(9)	501(7)	8001(5)	41(3)
N(100)	−4193(6)	−2197(6)	4336(4)	33(2)	O(203)	−4168(5)	402(4)	8785(3)	30(2)
C(101)	−4235(8)	−1102(7)	4205(6)	43(3)	C(204)	−3472(8)	1354(7)	9238(6)	37(2)
C(102)	−3585(8)	−307(7)	4871(6)	45(3)	C(205)	−3419(8)	1296(7)	10037(6)	43(3)
O(103)	−2321(5)	−328(4)	5123(3)	32(2)	O(206)	−2795(5)	489(4)	10324(3)	30(2)
C(104)	−1699(9)	309(7)	5823(6)	43(3)	C(207)	−2727(8)	421(7)	11081(5)	39(3)
C(105)	−380(9)	377(7)	6009(5)	39(2)	C(208)	−1886(8)	−321(7)	11390(5)	36(2)
C(106)	−129(6)	−632(5)	6134(3)	37(2)	N(209)	−2272(6)	−1390(6)	11014(4)	27(2)
C(107)	1136(9)	−610(7)	6338(5)	47(3)	C(210)	−3296(8)	−1952(8)	11260(5)	38(2)
C(108)	1356(9)	−1674(8)	6566(5)	47(3)	C(211)	−3969(8)	−2996(8)	10781(5)	41(3)
N(109)	843(6)	−2549(6)	5954(4)	34(2)	O(212)	−4557(5)	−2811(4)	10032(4)	32(2)
C(110)	737(9)	−3562(7)	6277(6)	52(3)	C(213)	−5163(9)	−3779(7)	9536(6)	41(3)
C(111)	−462(9)	−3879(8)	6450(6)	46(3)	C(214)	−5863(8)	−3553(8)	8815(5)	41(3)
O(112)	−1416(6)	−4137(5)	5759(4)	43(2)	O(215)	−5063(5)	−2934(4)	8473(3)	31(2)
C(113)	−2560(10)	−4684(8)	5849(6)	55(3)	C(216)	−5629(8)	−2884(7)	7714(5)	41(3)
C(114)	−3160(10)	−3964(8)	6179(6)	50(3)	C(217)	−4704(9)	−2379(8)	7359(5)	42(3)

Table 6 (Continued)

	x	*y*	*z*	U_{eq}		*x*	*y*	*z*	U_{eq}
				$K^+(2,2,2\text{-crypt-}K^+)_2HOSnTe_3^{3-}$ (Continued)					
O(115)	−3488(5)	−3166(5)	5740(4)	40(2)	C(218)	−2990(8)	−988(7)	7439(5)	35(2)
C(116)	−4638(8)	−3469(7)	5217(5)	40(3)	C(219)	−1957(8)	−1543(8)	7730(5)	39(3)
C(117)	−4972(8)	−2547(7)	4820(6)	40(3)	O(220)	−1452(5)	−1323(4)	8506(3)	28(1)
C(118)	−4622(8)	−2894(8)	3615(5)	39(3)	C(221)	−603(7)	−1991(7)	8781(5)	32(2)
C(119)	−3721(8)	−2805(7)	3180(5)	37(2)	C(222)	−8(7)	−1685(7)	9595(5)	32(2)
O(120)	−2646(5)	−3135(4)	3598(3)	29(1)	O(223)	−876(5)	−1939(4)	10007(3)	27(1)
C(121)	−1820(8)	−3198(7)	3175(5)	37(2)	C(224)	−313(7)	−1626(7)	10795(5)	28(2)
C(122)	−770(8)	−3588(7)	3616(5)	33(2)	C(225)	−1222(7)	−1930(7)	11213(5)	31(2)
				$K^+(2,2,2\text{-crypt-}K^+)_2HOSnTe_3^{3-}\cdot$en					
Sn(1)	20219(1)	−18494(1)	12954(1)	46(1)	C(125)	24455(16)	−27621(12)	12275(12)	101(6)
Te(1)	19854(1)	−17618(1)	14274(1)	65(1)	K(2)	17701(2)	−22152(2)	12414(2)	51(1)
Te(2)	22284(1)	−19591(1)	12276(1)	63(1)	N(200)	17306(12)	−23453(9)	11722(9)	83(4)
Te(3)	18891(1)	−17523(1)	11921(1)	75(1)	C(201)	17151(15)	−22950(13)	10851(11)	88(5)
O(1)	19834(6)	−19677(6)	13718(5)	57(2)	C(202)	17940(17)	−22570(15)	10314(11)	111(7)
K(3)	18580(3)	−19455(3)	15352(2)	97(1)	O(203)	17826(10)	−21783(1)	10661(7)	102(4)
K(1)	23168(2)	−24842(2)	11977(2)	51(1)	C(204)	18587(18)	−21435(18)	10146(13)	134(8)
N(100)	22847(8)	−22695(7)	11181(7)	56(3)	C(205)	18556(17)	−20610(14)	10430(11)	114(7)
C(101)	22057(12)	−22073(10)	11811(10)	76(4)	O(206)	18760(8)	−20915(7)	11241(6)	70(3)
C(102)	22267(13)	−22408(11)	12686(10)	80(5)	C(207)	18628(13)	−20112(11)	11548(10)	82(5)
O(103)	22298(7)	−23411(7)	13052(6)	66(3)	C(208)	18853(13)	−20464(12)	12414(10)	80(4)
C(104)	22626(14)	−23800(13)	13792(11)	87(5)	N(209)	18112(9)	−20838(8)	13095(7)	63(3)
C(105)	22426(14)	−24705(13)	14263(10)	95(6)	C(210)	18553(13)	−21437(10)	13853(9)	76(4)
O(106)	22998(8)	−25483(8)	13759(6)	82(3)	C(211)	19367(13)	−22422(12)	13697(11)	85(5)
C(107)	22763(15)	−26369(14)	14147(10)	105(6)	O(212)	18998(7)	−23061(7)	13561(6)	64(2)
C(108)	23559(14)	−27238(11)	13666(9)	88(5)	C(213)	19756(12)	−24017(11)	13454(11)	83(5)
N(109)	23495(10)	−26992(8)	12768(8)	74(3)	C(214)	19308(14)	−24657(11)	13348(11)	94(5)
C(110)	22605(18)	−27159(13)	12736(14)	123(7)	O(215)	18967(7)	−24239(6)	12599(6)	69(3)
C(111)	22285(18)	−26702(14)	11901(15)	128(8)	C(216)	18591(15)	−24878(11)	12490(13)	105(6)
O(112)	21901(8)	−25618(7)	11732(7)	76(3)	C(217)	18243(16)	−24407(12)	11647(13)	107(6)
C(113)	21567(13)	−25185(13)	10949(10)	81(5)	C(218)	16321(20)	−23595(18)	12339(14)	131(8)
C(114)	21160(11)	−24113(13)	10827(9)	75(4)	C(219)	15369(17)	−22555(19)	12557(16)	133(8)
O(115)	21954(6)	−23798(7)	10744(6)	58(2)	O(220)	15689(9)	−22212(10)	13031(8)	91(3)
C(116)	21623(12)	−22765(12)	10529(10)	80(5)	C(221)	14839(15)	−21361(18)	13328(15)	130(8)
C(117)	22483(12)	−22435(10)	10419(9)	70(4)	C(222)	15088(14)	−20969(18)	13913(15)	136(8)
C(118)	23869(13)	−22586(11)	10938(10)	83(5)	O(223)	15963(8)	−20678(8)	13399(7)	92(3)
C(119)	24787(13)	−23399(13)	10531(10)	80(5)	C(224)	16143(16)	−20276(14)	13960(13)	113(6)
O(120)	24936(7)	−24294(8)	11130(6)	68(3)	C(225)	17093(16)	−19967(11)	13381(12)	104(6)
C(121)	25883(12)	−25067(13)	10781(12)	84(5)	N(300)	17073(17)	−17922(14)	14462(14)	185(9)
C(122)	26016(11)	−25962(17)	11457(13)	112(8)	C(301)	16019(26)	−17099(27)	14665(29)	404(32)
O(123)	25218(7)	−26389(7)	11590(6)	74(3)	C(302)	15830(23)	−16088(23)	14162(25)	274(18)
C(124)	25378(15)	−27380(12)	12111(11)	102(6)	N(303)	16597(35)	−15700(23)	13602(29)	519(36)

[a] U_{eq} defined as one-third of the trace of the orthogonalized $\boldsymbol{U}_{ij}$ tensor.

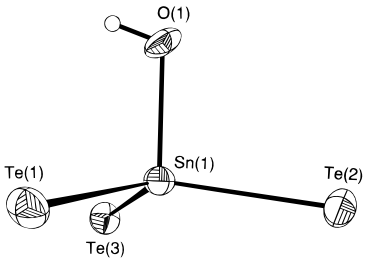

Figure 6. ORTEP view of $HOSnTe_3^{3-}$ in $K^+(2,2,2\text{-crypt-}K^+)_2HOSnTe_3^{3-}$ (**4**). Thermal ellipsoids are shown at the 50% probability level.

eight modes are infrared active (B_{1u}, B_{2u}, and B_{3u}), and the A_u mode is inactive.

The Raman spectrum of $Sn_2Se_6^{4-}$ has been reported for $Na_4Sn_2Se_6\cdot13H_2O$[87] and is in agreement with the anion frequencies in both $(enH^+)_2(2,2,2\text{-crypt-}K^+)_2Sn_2Se_6^{4-}$ and $K^+(N(CH_3)_4^+)_3Sn_2Se_6^{4-}$. However, only six of the possible nine Raman-active anion modes could be observed for $Na_4Sn_2Se_6\cdot13H_2O$, and only the totally symmetric modes, $\nu_1(A_g)$ and $\nu_2(A_g)$, were assigned.[87] An unassigned Raman spectrum of $Sn_2S_6^{4-}$ in $Na_4Sn_2S_6\cdot14H_2O$ has also been reported.[88]

The $Sn_2Se_6^{4-}$ vibrational modes have been assigned by analogy with Ga_2Br_6,[83] for which both the infrared and Raman spectra, including Raman polarization measurements, have been obtained, and the assignments have been confirmed by a normal-coordinate analysis.[89] With the exception of $\nu_2(A_g)$ for $Ge_2S_6^{4-}$ and $\nu_2(A_g)$ and $\nu_3(A_g)$ for $Ge_2Se_6^{4-}$, the assignments of the anion vibrational modes in $Na_4Ge_2S_6\cdot14H_2O$[65] and in $Na_4Ge_2Se_6\cdot16H_2O$[76] are at variance with our assignments, which are based on a previously reported normal-coordinate analysis of Ga_2Cl_6[89] and therefore are reassigned in Table 8. Factor-group analyses have also been performed using the site symmetries of the $Sn_2Se_6^{4-}$anions within the primitive unit cells and are taken as C_1 for $K^+(N(CH_3)_4^+)_3Sn_2Se_6^{4-}$ and as C_i for $(enH^+)_2(2,2,2\text{-crypt-}K^+)_2Sn_2Se_6^{4-}$. The correlations are given in Table 10 and indicate that all 18 modes of the $Sn_2Se_6^{4-}$ anion in $K^+(N(CH_3)_4^+)_3Sn_2Se_6^{4-}$ have A_g symmetry under C_i crystal symmetry and are Raman active. In the case of $(enH^+)_2(2,2,2\text{-crypt-}K^+)_2Sn_2Se_6^{4-}$, each Raman band of the anion is split into an A_g and a B_g component (A_u and B_u in the infrared spectrum) under C_{2h} crystal symmetry. Only 13 of the possible 18 Raman bands are observed for $K^+(N(CH_3)_4^+)_3Sn_2Se_6^{4-}$, and the split-

(88) Krebs, B.; Pohl, S.; Schiwy, W. *Angew. Chem., Int. Ed. Engl.* **1970**, *9*, 897. Twelve bands were reported for the Raman spectrum of $Na_4Sn_2S_6\cdot14H_2O$: 391, 377, 341, 281, 190, 178, 151, 136, 118, 96, 59, 44 cm^{-1} (relative intensities not given).

(89) Adams, D. M.; Churchill, R. G. *J. Chem. Soc. A* **1970**, 697.

Table 7. Selected Bond Lengths (Å), Significant Long Contacts (Å), and Bond Angles (deg) for $K^+(N(CH_3)_4^+)_3Sn_2Se_6^{4-}$, $(enH^+)_2(2,2,2\text{-crypt-}K^+)_2Sn_2Se_6^{4-}$, $(K^+)_2(2,2,2\text{-crypt-}K^+)_2Sn_2Te_6^{4-}$, $K^+(2,2,2\text{-crypt-}K^+)_2HOSnTe_3^{3-}$, and $K^+(2,2,2\text{-crypt-}K^+)_2HOSnTe_3^{3-}\cdot$en

$K^+(N(CH_3)_4^+)_3Sn_2Se_6^{4-}$		$(enH^+)_2(2,2,2\text{-crypt-}K^+)_2Sn_2Se_6^{4-}$	
Sn(1)−Se(1)	2.603(2)	Sn(1)−Se(1)	2.467(1)
Sn(1)−Se(1A)	2.580(2)	Sn(1)−Se(2)	2.452(1)
Sn(1)−Se(2)	2.467(2)	Sn(1)−Se(3)	2.570(1)
Sn(1)−Se(3)	2.471(2)	Sn(1)−Se(3A)	2.594(1)
Sn(1)···Sn(1A)	3.554(2)	Sn(1)···Sn(1A)	3.557(1)
Sn(2)−Se(4)	2.606(2)		
Sn(2)−Se(4A)	2.601(2)		
Sn(2)−Se(5)	2.444(2)		
Sn(2)−Se(6)	2.456(2)		
Sn(2)···Sn(2A)	3.602(3)		
K···Se(2)	3.369(3)	N(200)···Se(1)	3.374(5)
K···Se(3)	3.333(3)	N(200)···Se(2)	3.432(5)
K···Se(4)	3.692(3)	N(200) c··Se(3)	3.735(5)
K···Se(5)	3.330(3)	N(200)···Se(1A)	3.484(4)
K···Se(6)	3.326(3)	N(200)···Se(2A)	3.570(4)
Sn(1)−Se(1)−Sn(1A)	86.58(5)	Sn(1)−Se(3)−Sn(1A)	87.05(2)
Se(1)−Sn(1)−Se(1A)	93.42(5)	Se(3)−Sn(1)−Se(3A)	92.95(2)
Sn(2)−Se(4)−Sn(2A)	87.54(5)		
Se(4)−Sn(2)−Se(4A)	92.46(5)		

$(K^+)_2(2,2,2\text{-crypt-}K^+)_2Sn_2Te_6^{4-}$			
Sn(1)−Te(1)	2.820(3)	Sn(1)···Sn(1A)	3.865(3)
Sn(1)−Te(1A)	2.814(3)	K(2)···Te(1)	3.580(11)
Sn(1)−Te(2)	2.674(3)	K(2)···Te(2)	3.719(11)
Sn(1)−Te(3)	2.664(3)	K(2)···Te(3)	3.778(11)
Sn(1)−Te(1)−Sn(1A)	86.59(9)	Te(1)−Sn(1)−Te(1A)	93.41(9)

$K^+(2,2,2\text{-crypt-}K^+)_2HOSnTe_3^{3-}$		$K^+(2,2,2\text{-crypt-}K^+)_2HOSnTe_3^{3-}\cdot$en	
Sn(1)−Te(1)	2.710(1)	Sn(1)−Te(1)	2.699(1)
Sn(1)−Te(2)	2.705(1)	Sn(1)−Te(2)	2.707(2)
Sn(1)−Te(3)	2.674(1)	Sn(1)−Te(3)	2.683(2)
Sn(1)−O(1)	2.081(5)	Sn(1)−O(1)	2.027(8)
Te(1)−Sn(1)−Te(2)	116.71(3)	Te(1)−Sn(1)−Te(2)	114.54(5)
Te(1)−Sn(1)−Te(3)	116.25(3)	Te(1)−Sn(1)−Te(3)	117.38(5)
Te(2)−Sn(1)−Te(3)	118.21(3)	Te(2)−Sn(1)−Te(3)	119.82(5)
O(1)−Sn(1)−Te(1)	96.1(2)	O(1)−Sn(1)−Te(1)	96.2(2)
O(1)−Sn(1)−Te(2)	96.1(2)	O(1)−Sn(1)−Te(2)	96.9(2)
O(1)−Sn(1)−Te(3)	107.6(2)	O(1)−Sn(1)−Te(3)	105.5(2)

tings of the Raman-active anion bands in $(enH^+)_2(2,2,2\text{-crypt-}K^+)_2Sn_2Se_6^{4-}$ are too small to be resolved.

The $Sn_2Se_6^{4-}$ anion modes are shifted to lower frequency relative to those of $Ge_2S_6^{4-}$ and $Ge_2Se_6^{4-}$ by virtue of the reduced mass effect. As in $Ge_2Ch_6^{4-}$ (Ch = S, Se) and $Sn_2S_6^{4-}$, the most intense peak (202 cm^{-1}) in the $(enH^+)_2(2,2,2\text{-crypt-}K^+)_2$ salt was assigned to the symmetric ring mode $\nu_2(A_g)$. The symmetric terminal Sn−Se stretching mode, $\nu_1(A_g)$, is expected to be similar to the symmetric stretching mode, $\nu_1(A_1)$, of $SnSe_4^{4-}$ (239, 247 cm^{-1})[46] and was assigned to the band at 248 cm^{-1}. A similar trend is noted for $Ge_2S_6^{4-}$ (416 cm^{-1})[68] and GeS_4^{4-} (417 cm^{-1}).[90] The symmetric deformation mode, $\nu_3(A_g)$, of the terminal $SnSe_2$ groups was assigned to the line at 118 cm^{-1}. The ring deformation mode, $\nu_4(A_g)$, was assigned to the line at 74 cm^{-1}. The asymmetric Sn−Se stretching mode, $\nu_6(B_{1g})$, is expected to be weak in the Raman spectrum and likely overlaps with the terminal $SnSe_2$ bending mode, $\nu_{15}(B_{3g})$, at 179 cm^{-1}. The highest frequency band at 270 cm^{-1} was assigned to the asymmetric Sn−Se terminal stretching mode, $\nu_{11}(B_{2g})$. The remaining torsional modes, $\nu_7(B_{1g})$ and $\nu_{12}(B_{1g})$, were assigned to bands at 104 (14) and 87 (8) cm^{-1}, respectively. While the A_g, B_{1g}, B_{2g}, and B_{3g} anion modes of the $K^+(N(CH_3)_4^+)_3$ salt are in agreement with those of the $(enH^+)_2(2,2,2\text{-crypt-}K^+)_2$ salt, additional modes observed in the Raman spectrum of the $K^+(N(CH_3)_4^+)_3$ salt were assigned to the formally Raman-inactive (infrared-active) anion modes $\nu_5(A_u)$, $\nu_8(B_{1u})$, $\nu_9(B_{1u})$, $\nu_{13}(B_{2u})$, $\nu_{14}(B_{2u})$, $\nu_{16}(B_{3u})$, $\nu_{17}(B_{3u})$, and $\nu_{18}(B_{3u})$, which become Raman active under C_i crystal symmetry. Tentative assignments based on the frequency ordering of the infrared-active modes in Ga_2Br_6 are given in Table 8.

The spectrum of the $Sn_2Te_6^{4-}$ anion consists of several overlapping bands and is attributed to the similarity in the masses of tin and tellurium. Moreover, because of the small mass difference, the vibrational modes are expected to be even more strongly coupled than in $Sn_2Se_6^{4-}$ and $Ge_2S_6^{4-}$. A factor-group analysis has been performed using the site symmetry, C_i, of the $Sn_2Te_6^{4-}$ anions within the primitive unit cell. The appropriate correlations are given in Table 10 and indicate that each Raman band of the anion correlates to A_g symmetry and each infrared band to A_u symmetry under C_i crystal symmetry so that no factor-group splitting is expected in either the Raman or the infrared spectrum. Tentative assignments (Table 9) have been made by analogy with the $Sn_2Se_6^{4-}$ anion and isoelectronic In_2I_6;[84] the latter has been fully assigned on the basis of a normal-coordinate analysis.[89] Because of the reduced mass effect, the vibrational modes of the $Sn_2Te_6^{4-}$ anion occur at lower frequency than those of the $Sn_2Se_6^{4-}$ anion. The most intense peak at 134 cm^{-1} was assigned to the symmetric ring mode, $\nu_2(A_g)$, and the totally symmetric Sn−Te stretching mode, $\nu_1(A_g)$, was assigned to the Raman band at 185 cm^{-1}. The highest frequency band at 196 cm^{-1} was assigned to the asymmetric Sn−Te stretching mode, $\nu_{11}(B_{2g})$, and an intense shoulder at 121 cm^{-1} was assigned to $\nu_{15}(B_{3g})$. The remaining assignments for $\nu_3(A_g)$, $\nu_4(A_g)$, $\nu_6(B_{1g})$, $\nu_7(B_{1g})$, and $\nu_{12}(B_{2g})$ are deemed more tentative.

Conclusion

The molecular structures of the $Sn_2Ch_6^{4-}$ (Ch = Se, Te) and $Sn_2Te_7^{4-}$ anions have been known for some time. This paper reports the first characterization of the $Sn_2Ch_6^{4-}$, $Sn_2Te_7^{4-}$, and the novel $Sn_2Se_7^{4-}$ anions in solution by natural abundance ^{77}Se, ^{119}Sn, and ^{125}Te NMR spectroscopy. The solution structures were confirmed by a detailed analysis of the first-order ^{119}Sn NMR subspectra arising from natural abundance isotopomer distributions, and the $^1K(Sn-Ch_t)_{RC}$, $^1K(Sn-Ch_{mb})_{RC}$, and $^1K(Sn-Ch_{db})_{RC}$ coupling constants were shown to correlate with the Sn−Ch_t, Sn−Ch_{mb}, and Sn−Ch_{db} bond distances. Although previous NMR studies have systematically dealt with simple main-group polychalcogenide anions, the present findings represent the first multi-NMR speciation study of factors influencing condensation processes of simple polychalcogenide anions in nonaqueous solvents. The condensation equilibria among $SnCh_3^{2-}$ and the $Sn_2Ch_6^{4-}$, $Sn_2Ch_7^{4-}$, and $Sn_4Ch_{10}^{4-}$ anions were shown to be influenced by the relative amounts of uncryptated alkali-metal cations present in solution, establishing that oligomerization is promoted by ion-pair formation. The hydroxide derivative of the $SnTe_3^{2-}$ anion, $HOSnTe_3^{3-}$, was characterized in the solid state by X-ray crystallography and represents the second example of a simple mixed hydroxytelluride anion of a group 14 metal.

Experimental Section

Apparatus and Materials. All compounds used and prepared during the course of this work were air-sensitive. Consequently, all manipulations were carried out under rigorously anhydrous and oxygen-free conditions on a grease-free glass vacuum line equipped with glass/

(90) Pohl, S.; Schiwy, W.; Weinstock, N.; Krebs, B. *Z. Naturforsch.* **1973**, *B28*, 565.

Table 8. Raman Vibrational Frequencies and Assignments for the $Sn_2Se_6^{4-}$ Anion in $K^+(N(CH_3)_4^+)_3Sn_2Se_6^{4-}$ (**1**) and in $(enH^+)_2(2,2,2\text{-crypt-}K^+)_2Sn_2Se_6^{4-}$ (**2**) and the Related $Ge_2Ch_6^{4-}$ (Ch = S, Se) Anions and Ga_2X_6 (X = Cl, Br) Molecules

freq, cm^{-1}						freq, cm^{-1}	
Ga_2Cl_6[a]	$Ge_2S_6^{4-}$ [b]	Ga_2Br_6[c]	$Ge_2Se_6^{4-}$ [d]	$Sn_2Se_6^{4-}$ (**2**)[e]	assignt[f]	$Sn_2Se_6^{4-}$ (**1**)[e]	assignt[f]
462 (m)	433 (25)	339 (0.2)	306 (36)	270 (20)	$\nu_{11}(B_{2g})$	280 (13) 260 (12)	$\nu_{11}(B_{2g})$, $\nu_8(B_{1u})$
413 (s)	416 (20)	291 (1.5)	294 (21)	248 (25)	$\nu_1(A_g)$	255 (14) 249 (12)	$\nu_1(A_g)$, $\nu_{16}(B_{3u})$, $\nu_{13}(B_{2u})$
243 (w)		241 (0.2)	~250 (<1)	~185 (sh)	$\nu_6(B_{1g})$		
318 (mw)	372 (100)	204 (6)	207 (100)	202 (100)	$\nu_2(A_g)$	200 (100)	$\nu_2(A_g)$
215 (sh)	305 (22)	158 (0.2)		179 (15)	$\nu_{15}(B_{3g})$	178 (7) 173 (8)	$\nu_{15}(B_{3g})$, $\nu_{17}(B_{3u})$
167 (m)	205 (20)	119 (4)	139 (37)	118 (8)	$\nu_3(A_g)$	121 (4) 118 (6)	$\nu_3(A_g)$, $\nu_9(B_{1u})$
125 (sh)	198 (20)	85 (5.5)	121 (5)	104 (14)	$\nu_7(B_{1g})$	90 (11) 75 (13) 67 (10) 62 (7)	$\nu_4(A_g)$, $\nu_5(A_u)$, $\nu_7(B_{1g})$, $\nu_{12}(B_{2g})$, $\nu_{14}(B_{2u})$, $\nu_{18}(B_{3u})$
117 (w)	178 (38)	74 (10)		87 (8)	$\nu_{12}(B_{2g})$		
100 (s)	142 (33)	64 (?)		74 (14)	$\nu_4(A_g)$		

[a] References 82 and 83. [b] Reference 68. [c] Reference 84. [d] Reference 76; the weak line at ~250 cm^{-1} is not reported but is visible in the published trace of the spectrum. [e] Present work. [f] Assignments are made under D_{2h} point symmetry.

Table 9. Raman Vibrational Frequencies and Assignments for the $Sn_2Te_6^{4-}$ Anion in $(K^+)_2(2,2,2\text{-crypt-}K^+)_2Sn_2Te_6^{4-}$ and the Related In_2I_6 Molecule

In_2I_6[a]		$Sn_2Te_6^{4-}$ [c]	
freq, cm^{-1}	assignt[b]	freq, cm^{-1}	assignt[b]
232 (0.5)	$\nu_{11}(B_{2g})$	196 (15)	$\nu_{11}(B_{2g})$
187 (1.5)	$\nu_1(A_g)$	185 (8)	$\nu_1(A_g)$
134 (10)	$\nu_1(A_g)$	176 (3)	*d*
114 (0)	$\nu_6(B_{1g})$	147 (11, sh)	$\nu_6(B_{1g})$
69 (5)	$\nu_3(A_g)$	134 (100)	$\nu_2(A_g)$
55 (1)	$\nu_7(B_{1g})$	121 (25, sh)	$\nu_{15}(B_{3g})$
49 (8) 44 (6.5) 40 (0.5)	$\nu_{12}(B_{2g})$ $\nu_{15}(B_{3g})$ $\nu_4(A_g)$	92 (3) 82 (4) 71 (8)	$\nu_3(A_g)$, $\nu_4(A_g)$, $\nu_7(B_{1g})$, $\nu_{12}(B_{2g})$

[a] Reference 84. [b] Assignments are made under D_{2h} point symmetry. [c] Present work. [d] Unassigned mode.

Teflon stopcocks (J. Young Scientific Glassware), in a two-station nitrogen-atmosphere drybox (Vacuum Atmospheres Model DLX with moisture and oxygen levels <0.1 ppm; for general solid and crystal handling), or glovebag (for solution handling) which had been purged with dry nitrogen for at least 12 h prior to use.

Potassium metal (BDH Chemicals, >99%), stored under paraffin oil, was cleaned as previously described,[46] and freshly cut samples were handled only in the drybox. Tin shot (Baker Analyzed, 99.9%), tellurium powder (Alfa Inorganics, 99.9%), selenium powder (Alfa Inorganics, 99.9%), 2,2,2-crypt (4,7,13,16,21,24-hexaoxa-1,10-diazabicyclo[8.8.8]hexacosane; Merck, 99%, or Aldrich, 98%), and $N(CH_3)_4^+Br^-$ (BDH Chemicals, 98.5%) were used as received and dried in the evacuated port of the drybox for a minimum of 45 min, followed by exposure to the atmosphere of the drybox for at least 2 days prior to use.

All solvents were thoroughly dried, transferred by vacuum distillation, and stored in round-bottom flasks equipped with glass/Teflon stopcocks. Tetrahydrofuran (Aldrich, 99.9%) was stored over freshly cut sodium wire (BDH Chemicals, 99.8%). Methanol (Baker Analyzed HPLC Grade) was stored for 1 week over anhydrous $MgSO_4$ (Baker) before it was vacuum-distilled into a second round-bottom flask containing freshly-cut sodium metal. Ethylenediamine (Fisher Scientific Co., 99%) was dried over CaH_2 (BDH Chemicals) for several weeks and then vacuum-distilled onto, and stored over, fresh CaH_2 for at least an additional week prior to use. Anhydrous ammonia (Canadian Liquid Air or Matheson) was further dried over freshly cut sodium metal at −78 °C for at least 1 week prior to use.

Preparation of the Ternary Alloys. The M/Sn/Ch (M = Na, K, Tl; Ch = Se, Te) alloys were prepared as previously described[28] by fusion of the elements in the required molar ratios inside thick-walled Pyrex tubes. $KSnSe_2$: K, 0.9591 g, 24.53 mmol; Sn, 2.7575 g, 23.23 mmol; Se, 3.7318 g, 47.26 mmol. $KSnTe_2$: K, 1.0614 g, 27.15 mmol; Sn, 2.9595 g, 24.93 mmol; Te, 5.8893 g, 46.15 mmol. NaSnTe: Na, 0.1607 g, 6.99 mmol; Sn, 0.8242 g, 6.94 mmol; Te, 0.9050 g, 7.09 mmol. $Tl_2Sn_2Te_3$: Tl, 1.0790 g, 5.280 mmol; Sn, 0.6353 g, 5.353 mmol; Te, 1.0676 g, 8.367 mmol. The resulting alloys were ground into fine powders, and the compositions of the Na and K alloys were corrected for recovered tin lumps ($KSnSe_2$, 0.8151 g, 6.87 mmol; $KSnTe_2$, 0.9246 g, 7.79 mmol; NaSnTe, 0.4617 g, 3.97 mmol) to $KSn_{0.67}Se_{1.93}$, $KSn_{0.63}Te_{1.70}$, and $NaSn_{0.43}Te$. The compound K_2Te was prepared as described previously.[70]

KSnSe. The binary alloy KSn was initially prepared by fusing potassium metal (0.6328 g, 16.18 mmol) with tin metal (1.9979 g, 16.83 mmol), and in a second step, selenium (0.8778 g, 11.12 mmol) was added and the mixture was remelted. The resulting alloy was ground and its stoichiometry corrected for the recovered Sn lump (1.2339 g, 10.40 mmol) to $KSn_{0.40}Se_{0.68}$. An aqueous extraction of the crude ternary alloy was carried out. To one arm of a Pyrex H-shaped vessel, consisting of two glass tubes (14-mm o.d.) divided by a 7-mm medium-porosity frit, was added deionized water (ca. 10 mL) which had been degassed under dynamic vacuum. The alloy was added to the degassed water under the dry nitrogen atmosphere of a glovebag. The solution was agitated for several minutes and filtered over to the second arm of the H-tube, and the tube joining the two branches was sealed off. The water was evaporated under dynamic vacuum, and the resulting amorphous orange solid was dried under dynamic vacuum for 12 h at room temperature and stored in the drybox.

Preparation of $Sn_2Ch_6^{4-}$ and $Sn_2Ch_7^{4-}$ (Ch = Se, Te) Solutions for NMR Spectroscopy. The anions were prepared by extracting the K/Sn/Ch powdered alloys in en or liquid NH_3 for 2−5 weeks in the absence or in the presence of nonstoichiometric amounts of 2,2,2-crypt with respect to K^+. The final solutions were isolated for NMR spectroscopy as previously described:[28] $Sn_2Se_6^{4-}$ and $Sn_2Se_7^{4-}$ ($KSn_{0.67}Se_{1.93}$ 0.1696 g, 0.626 mmol; 2,2,2-crypt 0.1000 g, 0.266 mmol); $Sn_2Te_6^{4-}$ and $Sn_2Te_7^{4-}$ ($KSn_{0.63}Te_{1.70}$ 0.3892 g, 1.176 mmol).

Multinuclear Magnetic Resonance Spectroscopy. All NMR spectra were routinely obtained without locking (field drift < 0.1 Hz h^{-1}) on Bruker AC-300 (7.0463 T; ^{119}Sn and ^{125}Te) and AM-500 (11.744 T; ^{77}Se, ^{119}Sn, and ^{125}Te) pulse spectrometers using 10-mm probes broad-banded over the frequency ranges 13.968−121.497 and 23.276−202.460 MHz, respectively. The experimental parameters for ^{119}Sn and ^{125}Te NMR spectra recorded at 7.0463 T are given in square brackets. The spectrometer frequencies were 95.384 (^{77}Se), 186.504 [111.922] (^{119}Sn) and 157.792 [94.692] MHz (^{125}Te). Free-induction

Table 10. Correlation Diagrams[a] for the Vibrational Modes of the $Sn_2Ch_6^{4-}$ (Ch = S, Te) Anions in $K^+(N(CH_3)_4^+)_3Sn_2Se_6^{4-}$,[b] $(enH^+)_2(2,2,2\text{-crypt-}K^+)_2Sn_2Se_6^{4-}$,[c] and $(K^+)_2(2,2,2\text{-crypt-}K^+)_2Sn_2Te_6^{4-}$ [d]

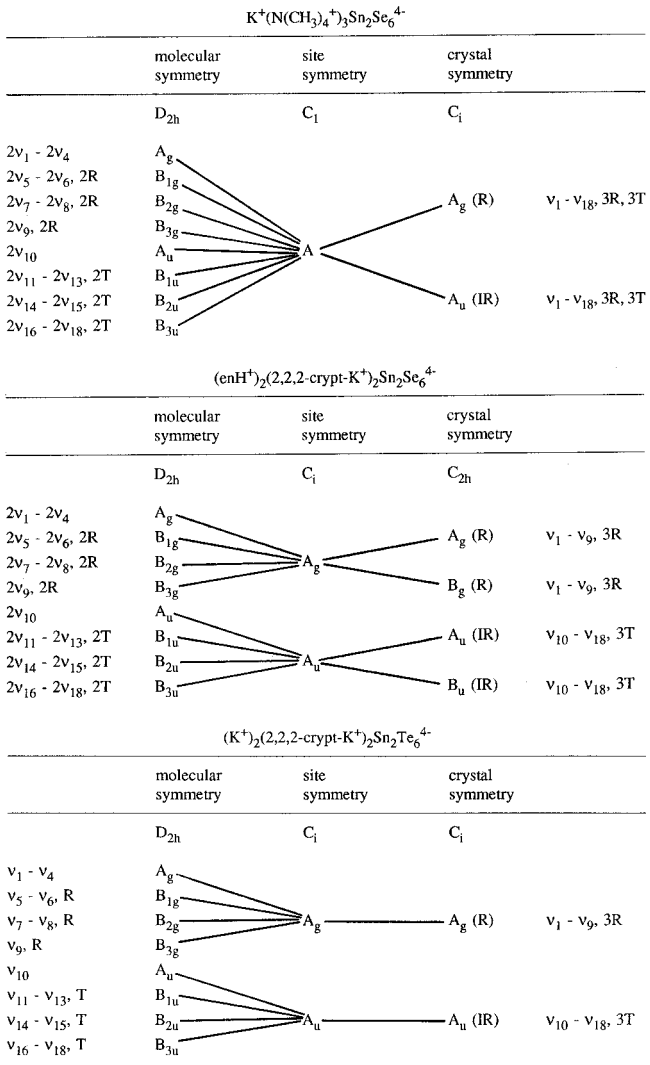

[a] R and T denote rotatory and translatory (external) modes, respectively. (R) and (IR) denote Raman and infrared activity, respectively. [b] Space group $P\bar{1}$, $Z = 2$. [c] Space group $P2_1/n$, $Z = 2$. [d] Space group $P\bar{1}$, $Z = 1$.

decays were typically accumulated in 16K or 32K memories. Spectral width settings of 25−100 kHz were employed, yielding data point resolutions of 3.05−6.10 Hz/data point and acquisition times of 0.328−0.164 s, respectively. Relaxation delays were not applied. Typically, 40 000−200 000 transients were accumulated depending on the concentrations and sensitivities of the nuclides under study. Pulse width settings corresponding to a bulk magnetization tip angle, θ, of ∼90° were 6 (^{77}Se), 15 [10] (^{119}Sn), and 18 [5] μs (^{125}Te). Line-broadening parameters used in the exponential multiplication of the free-induction decays were 20−30 Hz. Variable-temperature spectra were recorded using the variable-temperature controllers of the spectrometers, and temperatures (accurate to ±1.0 °C and stable to within ±0.10 °C) were checked by placing a copper−constantan thermocouple in the sample region of the probe. Samples were allowed to equilibrate for at least 5 min while spinning before spectral accumulations were begun.

The respective nuclei were referenced to neat samples of $(CH_3)_2Ch$ (Ch = Se, Te) and $(CH_3)_4Sn$ at 24 °C. The chemical shift convention used was a positive (negative) sign signifies a chemical shift to high (low) frequency of the reference compound.

The ^{119}Sn subspectra of the $Sn_2Ch_6^{4-}$ and $Sn_2Ch_7^{4-}$ (Ch = Se, Te) were simulated using the program DSYMPC.[91] Subspectra were weighted using the normalized total intensities listed in Tables 3 and 4 and summed using the Line Spectrum Addition subroutine in DYSMPC.

Raman Spectroscopy. Raman spectra were recorded on a Jobin-Yvon Mole S-3000 triple-spectrograph system equipped with a 0.32-m prefilter, adjustable 25-mm entrance slit, and a 1.00-m monochromator. Holographic gratings were used for the prefilter (600 grooves mm^{-1}, blazed at 500 nm) and monochromator (1800 grooves mm^{-1}, blazed at 550 nm) stages. An Olympus metallurgical microscope (model BHSm-L-2) was used for focusing the excitation laser to a 1-μm spot on the sample. The 514.5- ($Sn_2Se_6^{4-}$) and 647.1-nm lines ($Sn_2Te_6^{4-}$) of a Spectra Physics Model 2016 Ar^+ ion laser and a Lexel Laser Inc. Model 3500 Kr^+ ion laser, respectively, were used for the excitation of the sample. Spectra were recorded at ambient temperatures on powdered microcrystalline samples of $K^+(N(CH_3)_4^+)_3Sn_2Se_6^{4-}$ and $(K^+)_2(2,2,2\text{-crypt-}K^+)_2Sn_2Te_6^{4-}$ and crystals of $(enH^+)_2(2,2,2\text{-crypt-}K^+)_2Sn_2Se_6^{4-}$ sealed in baked-out Pyrex melting point capillaries. The powdered materials were obtained by carefully grinding several crystals inside the drybox using an agate mortar and pestle.

The spectra were recorded by signal averaging using a Spectraview-2D CCD detector equipped with a 25-mm chip (1152 × 298 pixels) and at a laser power of 150 mW for $K^+(N(CH_3)_4^+)_3Sn_2Se_6^{4-}$, 20 mW for $(enH^+)_2(2,2,2\text{-crypt-}K^+)_2Sn_2Se_6^{4-}$, and 100 mW for $(K^+)_2(2,2,2\text{-crypt-}K^+)_2Sn_2Te_6^{4-}$ and slit settings corresponding to 1 cm^{-1}. A total of 15 reads having 60 s integration times for $K^+(N(CH_3)_4^+)_3Sn_2Se_6^{4-}$ and $(K^+)_2(2,2,2\text{-crypt-}K^+)_2Sn_2Te_6^{4-}$ and 90 s integration times for $(enH^+)_2(2,2,2\text{-crypt-}K^+)_2Sn_2Se_6^{4-}$ were summed. Spectral line positions are estimated to be accurate to ±1 cm^{-1}.

Crystal Structure Determinations of $K^+(N(CH_3)_4^+)_3Sn_2Se_6^{4-}$ (1), $(enH^+)_2(2,2,2\text{-crypt-}K^+)_2Sn_2Se_6^{4-}$ (2), $(K^+)_2(2,2,2\text{-crypt-}K^+)_2Sn_2Te_6^{4-}$ (3), $K^+(2,2,2\text{-crypt-}K^+)_2HOSnTe_3^{3-}$ (4), and $K^+(2,2,2\text{-crypt-}K^+)_2HOSnTe_3^{3-}\cdot en$ (5). (a) Crystal Growing. $K^+(N(CH_3)_4^+)_3Sn_2Se_6^{4-}$ (1). The amorphous orange solid (0.2194 g) obtained by extracting $KSn_{0.40}Se_{0.68}$ in H_2O (*vide supra*) was dissolved in CH_3OH, producing an intense yellow solution. After 2 weeks, an excess of a saturated $N(CH_3)_4^+Br^-$ solution (0.0461 g, 0.299 mmol) in CH_3OH was carefully added to the yellow solution. After 3 days of standing, a large number of parallelepiped-shaped yellow crystals formed. The supernatant solution was removed from the reactor under the dry nitrogen atmosphere of a glovebag. The yellow crystals were dried under dynamic vacuum, transferred into a drybox equipped with a stereomicroscope, mounted, and sealed in 0.2 mm Lindemann glass capillaries.

$(enH^+)_2(2,2,2\text{-crypt-}K^+)_2Sn_2Se_6^{4-}$ (2). The extraction of $KSn_{0.67}Se_{1.93}$ (0.1269 g, 0.468 nmol) in en in the presence of a nonstoichiometric amount of 2,2,2-crypt (0.1500 g, 0.398 mmol) with respect to K^+ produced a deep yellow solution. The resulting solution was studied by ^{119}Sn and ^{77}Se NMR spectroscopy and revealed mainly the $SnSe_3^{2-}$ anion (77%) and small amounts of the $Sn_2Se_6^{4-}$ (16%) and $Sn_4Se_{10}^{4-}$ (7%) anions. The NMR sample was stored at room temperature for several months, during which a number of yellow platelike crystals formed. The crystals were isolated, dried under dynamic vacuum, transferred into the drybox, and mounted and sealed in 0.2 and 0.3 mm Lindemann glass capillaries.

$(K^+)_2(2,2,2\text{-crypt-}K^+)_2Sn_2Te_6^{4-}$ (3). The alloy $KSn_{0.63}Te_{1.70}$ (0.1494 g, 0.452 mmol) was transferred into one arm of a two-arm Pyrex vessel and extracted in en in the presence of a nonstoichiometric amount of 2,2,2-crypt (0.0684 g, 0.182 mmol) with respect to K^+. After 1 week, the deep red solution was carefully decanted off the alloy residue into the second arm of the reaction vessel. An excess of THF (1:2 v/v) was condensed under static vacuum at 0 °C into the first arm of the Pyrex reactor. The reactor was allowed to stand 2−3 weeks, over which the THF slowly vapor-phase-diffused into the en solution, resulting in the formation of deep red platelike crystals just above the supernatant. The mother liquor was decanted back into the first arm of the Pyrex vessel and removed under the dry nitrogen atmosphere of a glovebag. The crystalline sample was dried under dynamic vacuum at room temperature and transferred to the drybox where suitable single crystals were mounted and sealed in 0.2−0.3 mm Lindemann glass capillaries.

$K^+(2,2,2\text{-crypt-}K^+)_2HOSnTe_3^{3-}$ (4) and $K^+(2,2,2\text{-crypt-}K^+)_2HOSnTe_3^{3-}\cdot en$ (5). The reaction of the alloys $Tl_2Sn_2Te_3$ (0.1797 g,

(91) Hägele, G.; Höffken, H.-W.; Mistry, F.; Spiske, R.; Weber, U.; Goudetsidis, S. *DSYMPC*, Release 0.940728E; Institut für Anorganische Chemie and Strukturchemie, Heinrich-Heine-Universität: Düsseldorf, Germany, 1994.

0.175 mmol) and K_2Te (0.0522 g, 0.253 mmol) in en in the presence of a stoichiometric excess of 2,2,2-crypt (0.1958 g, 0.520 mmol) with respect to K^+ gave rise to a deep red solution which was shown by ^{119}Sn and ^{125}Te NMR spectroscopy to contain mainly the $TlSnTe_3^{3-}$ anions[78] and a new "Sn(IV)/Te_3" species (see **$HOSnTe_3^{3-}$ in 4 and 5**). As there was no evidence of crystallization in the NMR sample after several weeks, the solution was transferred into one arm of a two-arm Pyrex vessel under the dry nitrogen atmosphere of a glovebag. An excess of THF (1:2 v/v) was vacuum-distilled at 0 °C into the second arm of the Pyrex reactor. The vapor phase diffusion of the THF into the en solution over a period of 24 h led to the formation of deep red prisms of **5** whereas a complete intermixing of the solvents after a further 4 led to the formation of orange rectangular plates of **4**. Both crystal morphologies were isolated from the mother liquor as described above and dried under dynamic vacuum at room temperature. Suitable single crystals of both morphologies were mounted inside the drybox and sealed in 0.2 and 0.3 mm Lindemann glass capillaries.

The crystals used in this study had the following dimensions: 0.21 × 0.32 × 0.40 mm^3 (**1**), 0.49 × 0.45 × 0.13 mm^3 (**2**), 0.29 × 0.26 × 0.35 mm^3 (**3**), 0.39 × 0.19 × 0.28 mm^3 (**4**), and 0.43 × 0.21 × 0.30 mm^3 (**5**).

(b) Collection and Reduction of X-ray Data. All crystals were centered on a Syntex P3 diffractometer using silver radiation monochromatized with a graphite crystal (λ = 0.560 86 Å). During data collection, the intensities of three standard reflections were monitored every 97 reflections to check for crystal stabilities and alignments. No crystal decays were observed. For all compounds, corrections were made for Lorentz and polarization effects.

$K^+(NCH_3)_4^+)_3Sn_2Se_6^{4-}$ (1) and $(enH^+)_2$(2,2,2-crypt-$K^+)_2Sn_2Se_6^{4-}$ (2). The experimental values for **2**, when differing from those of **1**, are given in square brackets. Accurate cell dimensions were determined at 24 [−100] °C from a least-squares refinement of the setting angles (χ, ϕ, and 2θ) obtained from 17 [20] accurately centered reflections (with 22.61 [8.94]° ≤ 2θ ≤ 34.45 [28.90]°) chosen from a variety of points in reciprocal space. Integrated diffraction intensities were collected using a $\theta-2\theta$ [ω] scan technique with scan rates varying from 1.5 [3.0] to 14.6° min^{-1} in ω and a scan range of ±0.5 [±0.45]° so that weaker reflections were examined more slowly to minimize counting errors. Data were collected with 0 [0] ≤ h ≤ 11 [10], −12 [0] ≤ k ≤ 11 [31], −19 [−18] ≤ l ≤ 19 [17], and 4 [3]° ≤ 2θ ≤ 40°. A total of 6121 [6814] reflections were collected, of which 183 [219] were standard reflections. In total, 5585 [6010] unique reflections remained after averaging equivalent relfections. A total of 3152 [3908] reflections, satisfying the condition $I \geq 2\sigma(I)$, were used for the structure solution. Empirical absorption corrections were applied to both data sets using the ψ-scan method ($\Delta\phi$ = 10°, $\mu\bar{R}$ = 0.525 [0.420]).

$(K^+)_2$(2,2,2-crypt-$K^+)_2Sn_2Te_6^{4-}$ (3). Accurate cell dimensions were determined at 24 °C as described above from 35 accurately centered reflections [with 15.01° ≤ 2θ ≤ 23.06°] chosen from a variety of points in reciprocal space. Integrated diffraction intensities were collected using an ω-scan technique (scan rates 1.5−14.5° min^{-1} in ω; scan range ±0.40°). Data collection parameters were 0 ≤ h ≤ 11, −11 ≤ k ≤ 11, −18 ≤ l ≤ 17, and 3° ≤ 2θ ≤ 35°. A total of 5273 reflections were collected, of which 84 were standards. A total of 4555 unique reflections remained after averaging equivalent reflections, and a total of 2286 reflections, satisfying the condition $I \geq 2\sigma(I)$, were used for structure solution.

K^+(2,2,2-crypt-$K^+)_2HOSnTe_3^{3-}$ (4) and K^+(2,2,2-crypt-$K^+)_2$-$HOSnTe_3^{3-}$·en (5). The experimental values of **5**, when different from those of **4**, are given in square brackets. Accurate cell dimensions were determined at −105 [24] °C from 43 [36] accurately centered reflections (with 9.76 [7.24]° ≤ 2θ ≤ 27.30 [27.73]°) chosen from a variety of points in reciprocal space. Integrated diffraction intensities were collected using a $\theta-2\theta$ scan technique (scan rates 1.4 [3.5]−14.6° min^{-1}; scan range ±0.5°). The data were recorded with 0 [0] ≤ h ≤ 14 [18], −15 [−14] ≤ k ≤ 15 [16], −22 [−16] ≤ l ≤ 21 [17], and 3° ≤ 2θ ≤ 40°. A total of 10 995 [8907] reflections were collected, of which 355 [279] were standard reflections. A total of 10 109 [8256] unique reflections remained after averaging equivalent reflections, and a total of 5984 [4619] reflections, satisfying the condition $I > 2\sigma(I)$, were used for structure solution. Absorption corrections were applied using the program DIFABS.[92]

(c) Solution and Refinement of the Structures. All calculations were performed on a Silicon Graphics, Inc., Model 4600PC workstation using the SHELXTL PLUS package[93] for structure determination, refinement, and molecular graphics.

$K^+(N(CH_3)_4^+)_3Sn_2Se_6^{4-}$ (1), $(enH^+)_2$(2,2,2-crypt-$K^+)_2Sn_2Se_6^{4-}$ (2), and $(K^+)_2$(2,2,2-crypt-$K^+)_2Sn_2Te_6^{4-}$ (3). The original cells were first confirmed using the XPREP program[93] which showed the lattices to be primitive triclinic for **1** and **3** and primitive monoclinic for **2**. The structures were solved in the $P\bar{1}$ (**1** and **3**) and $P2_1/n$ (**2**) space groups which confirmed the presence of the $Sn_2Ch_6^{4-}$ (Ch = Se, Te) anions and the K^+, 2,2,2-crypt-K^+, $N(CH_3)_4^+$, and enH^+ cations in the appropriate cells. For compound **3**, the positionally disordered 2,2,2-crypt-K^+ cations were modeled using the positions of a 2,2,2-crypt-K^+ cation from compound **2** and refined using a rigid-body refinement (FRAG in SHELXTL PLUS). The final structure solutions for **1** and **2** were obtained by using data that had been corrected for absorption and by introducing anisotropic thermal parameters for all non-hydrogen atoms, calculated values for the positions of the hydrogen atoms [d(C−H) = 0.96 Å; d(N−H) = 0.90 Å; U(H) fixed to 1.2 × U(C) or U(N)], and weighting factors ($w = 1/[\sigma^2(F_o^2) + (0.0633P)^2 + 0.00P]$ for **1** and $1/[\sigma^2(F_o^2) + (0.0559P)^2 + 0.00P]$ for **2** where $P = [\max(F_o^2,0) + 2F_c]/3$), which gave rise to R_1 (wR_2) residuals of 0.0494 (0.1223) for **1** and 0.0396 (0.0918) for **2**. For compound **3**, the final structure solution was obtained without absorption corrections and by introducing anisotropic thermal parameters for the Sn, Te, and K atoms, calculated values for the positions of the hydrogen atoms, and a weighting factor ($w = 1/[\sigma^2(F_o^2) + (0.2669P)^2 + 0.00P]$); R_1 (wR_2) = 0.1172 (0.2961). The maximum (minimum) electron densities were 1.368 (−0.792), 0.868 (−0.746), and 2.159 (−1.562) e $Å^{-3}$ for **1**−**3**, respectively.

K^+(2,2,2-crypt-$K^+)_2HOSnTe_3^{3-}$ (4). The volume of the unit cell, 2641(1) $Å^3$, suggested the presence of four 2,2,2-crypt-K^+ cations.[94] The en solution from which the crystals were obtained had been shown by ^{119}Sn and ^{125}Te NMR spectroscopy to contain the $Tl_2Te_2^{2-}$, $SnTe_3^{2-}$, and HTe^- anions as minor species in solution along with large amounts of the $TlSnTe_3^{3-}$ anion and an unidentified species containing "Sn(IV)/Te" units (see **$HOSnTe_3^{3-}$ in 4 and 5**). The initial model used for the refinement of the structure involved four 2,2,2-crypt-K^+ cations and two $SnTe_3^{2-}$ anions. The XPREP program[93] confirmed the original cell and showed the lattice to be primitive triclinic (R_{int} = 0.017). The E statistics (calculated 0.933; theoretical 0.968) indicated a centrosymmetric structure. Consequently, the structure was solved in the $P\bar{1}$ space group.

The first solution was obtained without absorption corrections by conventional direct methods which located the general positions of one tin and three tellurium atoms and the general positions of all non-hydrogen atoms of two 2,2,2-crypt-K^+ cations. The Sn and Te atoms comprised a trigonal-pyramidal $SnTe_3$ group, contrasting with the trigonal-planar geometry of the $SnTe_3^{2-}$ anion established from solution multi-NMR and Mössbauer studies.[28] The full-matrix least-squares refinement of the positions and isotropic thermal parameters of the atoms gave a conventional agreement index, R_1, of 0.1388 and confirmed the presence of an $SnTe_3$ unit having C_{3v} point symmetry. An examination of the difference map revealed the presence of two additional peaks corresponding to 9.29 and 21.92 electrons. The weaker peak was located 2.16 Å from the tin atom and was perpendicular to the plane containing the three tellurium atoms. The stronger peak was independently located and was assigned to an uncryptated-K^+ cation, implying that the anion should possess a 3− charge. The weaker peak was consequently assigned to an O atom of an OH^- group by analogy with the structure of the $HOGeS_3^{3-}$ anion,[81] giving rise to the $HOSnTe_3^{3-}$ anion. The successive full-matrix least-squares refinement of the positions and isotropic thermal parameters of all the atoms produced a significant improvement in R_1 (0.0744) and confirmed the

(92) Walker, N.; Stuart, D. *Acta Crystallogr*. **1983**, *A39*, 158.

(93) Sheldrick, G. M. *SHELXTL PLUS*, Release 4.21/V; Siemens Analytical X-ray Instruments Inc.: Madison, WI, 1993.

(94) The unit cell volume of a structure containing 2,2,2-crypt-K^+ can provide a reliable count of the number of cations present in the unit cell and hence the charge on the anion(s) by assuming (a) an empirical volume of ca. 650 $Å^3$ for the 2,2,2-crypt-K^+ cation[19] and (b) that the crystal packing is dominated by the 2,2,2-crypt-K^+ cations.

presence of an uncryptated-K^+ cation and the $HOSnTe_3^{3-}$ anion. The introduction of the positions and anisotropic thermal parameters for all non-hydrogen atoms as well as the calculated values of the positions of the hydrogen atoms [d(C−H) = 0.96 Å; d(O−H) = 0.82 Å; U(H) fixed to 1.2 × U(C) or U(O)] resulted in a residual, R_1, of 0.0552.

The structure was solved a second time using data that had been corrected for absorption. The final refinement was obtained by introducing anisotropic thermal parameters for all non-hydrogen atoms and a weighting factor ($w = 1/[\sigma^2(F_o^2) + (0.0163P)^2 + 0.00P]$) and gave rise to a residual, R_1, of 0.0554 (wR_2 of 0.0762). In the final difference Fourier map, the maximum and minimum electron densities were 1.065 and −0.862 e Å^{-3}.

K^+(2,2,2-crypt-K^+)$_2HOSnTe_3^{3-}$·en (5). The volume of the unit cell, 3031(2) Å^3, suggested the presence fo five 2,2,2-crypt-K^+ cations. However, in light of the structure of compound **4**, the initial model used in the refinement of the structure involved four 2,2,2-crypt-K^+ cations, one K^+ cation, and one $HOSnTe_3^{3-}$ anion. The XPREP program confirmed the original cell and showed the lattice to be primitive triclinic (R_{int} = 0.020). The structure was solved in the $P\bar{1}$ space group (E statistics: calculated, 0.928; theoretical, 0.968).

The first structure solution was obtained without absorption corrections by conventional Patterson methods which located the general positions of one tin and three tellurium atoms of an $SnTe_3$ unit having a trigonal-pyramidal (C_{3v}) geometry. Successive difference Fourier syntheses revealed the general positions of all the non-hydrogen atoms of two 2,2,2-crypt-K^+ cations and confirmed the presence of a K^+ cation and an $HOSnTe_3^{3-}$ anion (R_1 = 0.1198). The introduction of the anisotropic thermal parameters for the Sn, Te, and K atoms as well as the calculated values of the positions of the hydrogen atoms located the general positions of an en solvent molecule [d(C−H) = 0.96 Å; d(N−H) = 0.90 Å; U(H) fixed to 1.2 × U(C) or U(N)]. All non-hydrogen atoms, except those comprising the en molecule, were refined anisotropically, producing a significant improvement in the structure (R_1 = 0.0552).

The structure was solved a second time using data that had been corrected for absorption. The final refinement was obtained by fixing the bond lengths and angles of the en solvent molecule and by introducing anisotropic thermal parameters for all non-hydrogen atoms and a weighting factor ($w = 1/[\sigma^2(F_o^2) + (0.0931P)^2 + 0.00P]$) and gave rise to a residual, R_1 (wR_2), of 0.0554 (0.1620). In the final difference Fourier map, the maximum and minimum electron densities were 2.538 and −0.666 e Å^{-3}.

Acknowledgment. We thank the Natural Sciences and Engineering Research Council of Canada for support in the form of an operating grant (G.J.S.) and for the award of a graduate scholarship (J.C.) and the German Academic Exchange Service (DAAD) for the award of a travel grant (M.G.). We also gratefully acknowledge David P. DiCiommo for his assistance in the preparation of the M/Sn/Ch (M Na, K) alloys and growing crystals of the compound $K^+(N(CH_3)_4^+)_3Sn_2Se_6^{4-}$.

Supporting Information Available: Structure determination parameters (Table S1), the remaining distances and angles in the $N(CH_3)_4^+$ and 2,2,2-crypt-K^+ cations (Table S2), anisotropic thermal parameters (Table S3), and atomic coordinates for the hydrogen atoms (Table S4) (31 pages). Ordering information is given on any current masthead page.

IC950917C